On the *in-vivo* photochemical rate parameters for PDT reactive oxygen species modeling

Michele M. Kim[1,2], **Ashwini A. Ghogare**[3,4], **Alexander Greer**[3,4], and **Timothy C. Zhu**[1]

[1]Department of Radiation Oncology, University of Pennsylvania, Philadelphia, PA

[2]Department of Physics and Astronomy, University of Pennsylvania, Philadelphia, PA

[3]Department of Chemistry, Graduate Center, City University of New York, Brooklyn College. Brooklyn, New York 11210, United States

[4]Ph.D. Program in Chemistry, The Graduate Center of the City University of New York, 365 Fifth Avenue, New York, New York 10016, United States

Abstract

Photosensitizer photochemical parameters are crucial data in accurate dosimetry for photodynamic therapy (PDT) based on photochemical modeling. Progress has been made in the last few decades in determining the photochemical properties of commonly used photosensitizers (PS), but mostly in solution or *in-vitro*. Recent developments allow for the estimation of some of these photochemical parameters *in-vivo*. This review will cover the currently available *in-vivo* photochemical properties of photosensitizers as well as the techniques for measuring those parameters. Furthermore, photochemical parameters that are independent of environmental factors or are universal for different photosensitizers will be examined. Most photosensitizers discussed in this review are of the type II (singlet oxygen) photooxidation category, although type I photosensitizers that involve other reactive oxygen species (ROS) will be discussed as well. The compilation of these parameters will be essential for ROS modeling of PDT.

1 Introduction

Photodynamic therapy (PDT) is a treatment modality for malignant and non-malignant diseases that uses visible light to activate photosensitizers to generate cytotoxic oxygen species to kill cancer cells (Dougherty, 1993). PDT has been approved by the U.S. Food and Drug Administration for the treatment of microinvasive lung cancer, obstructing lung cancer, and obstructing esophageal cancer, as well as for premalignant actinic keratosis and age-related macular degeneration (Agostinis *et al.*, 2011a; Huang, 2005a; Pogue *et al.*, 2016; Simone *et al.*, 2012; Wilson and Patterson, 2008; Zhu and Finlay, 2008).

Photodynamic therapy is not only "dynamic" but also multifaceted. There are three principal components: photosensitizer, light, and oxygen, all of which interact on time scales relevant to a single treatment. The distribution of light is determined by the light source characteristics and the tissue optical properties. The tissue optical properties, in turn, are influenced by the concentration of photosensitizer and the concentration and oxygenation of the blood. The distribution of oxygen is altered by the photodynamic process, because it

consumes oxygen, thus effecting the ingress of oxygen diffusion into tissue. The distribution of photosensitizer can be modeled as a diffusion process through the vasculature for most photosensitizers. Some, such as 5-aminolevulinic acid (ALA), induce the production of protoporphyrin IX (PpIX), which is governed by the concentration of free heme (Kennedy and Pottier, 1992). Finally, distribution of the photosensitizer may change as a result of photobleaching, which is the photodynamic destruction of the photosensitizer itself. To account for these interactions, a dynamic model of the photodynamic process is required.

Two types of photosensitized oxidation, named type I and type II, have emerged, as shown in figure 1 (Foote, 1976; Greer, 2006; Adam, 1981; Ranby, 1981; Foote, 1991). Both reactions involve the absorption of light by a photosensitizer ($[S_0]$) to produce an excited-state photosensitizer ($[S_1]$) (Foote, 1991).

The type I mechanism involves radicals or radical ions through hydrogen atom or electron transfer, yielding radicals or radical ions (Greer, 2006; Foote, 1991). The triplet state photosensitizer can also react directly with an organic molecule or substrate, but this is not classified as a photosensitized oxidation. Here, the substrate can donate an electron to the photosensitizer, creating a substrate radical cation and a photosensitizer radical anion (Simone *et al.*, 2012). This process can occur in hypoxic conditions, but in the presence of oxygen, the triplet photosensitizer undergoes electron transfer with molecular oxygen to generate superoxide anions ($O_2-\cdot$) (Sharman *et al.*, 2000). The radicals formed can react with each other or other molecules present (such as the molecular target or the solvent) to form other radical species leading to secondary reactions and the production of oxygenated compounds (Simone *et al.*, 2012; Sharman *et al.*, 2000; Gollnick, 1968). Superoxide anion is not very reactive in biological systems, but it can react with water to form hydrogen peroxide (H_2O_2). H_2O_2 easily passes through biological membranes, and since it is not restricted to one cellular component, it is quite relevant in causing cellular damage. Figure 2 shows the two pathways of a type I interaction – one via triplet state photosensitizer interact with $[A]$ directly without any oxygen mediation and one via an electron transfer to oxygen to form the superoxide anion ($O_2-\cdot$).

Most photosensitizers used in the clinic are of the type II category, which produce singlet oxygen as the main photocytotoxic agent for events that eventually cause cell death and/or therapeutic effects (Zhu and Finlay, 2008; Foote, 1976; Weishaupt *et al.*, 1976). In contrast to type I reactions, such as electron transfer to oxygen, in type II reactions, the photosensitizer triplet state, $[T_1]$, transfers energy to molecular oxygen to generate $^1O_2$. During PDT, as shown in figure 2, photosensitizer is excited by light at a certain wavelength matching the absorption energy gap to the excited state $[S_1]$ from its ground state $[S_0]$. Both this state and the ground state are spectroscopic singlet states. One essential property of a good photosensitizer is a high intersystem crossing (ISC) yield, i.e., a high probability of transition from (S_1) to a triplet state (T). In the T state, the photosensitizer can transfer energy to molecular oxygen ($^3O_2$), exciting it to its highly reactive singlet state ($^1O_2$). Ideal photosensitizer properties and experimental conditions that favor the singlet oxygen (type II) pathway include (i) a high extinction coefficient (ε), (ii) a high triplet quantum yield of the photosensitizer ($\Phi_t \sim 1$), and (iii) a low chemical reactivity of the photosensitizer triplet state ($k_8 \sim 0$). Competition between type I and II photooxidation chemistry is inevitable upon the

formation of an excited photosensitizer in the presence of $^3O_2$. Singlet oxygen ($^1O_2$) is a key reactive species produced in PDT, where estimates place the singlet oxygen contribution at ~80%, and hydroxyl radical and other reactive oxygen species at ~20% (Pouget *et al.*, 2000).

Photosensitizer properties and the concentration of oxygen present in the environment will be an important factor in determining the ratio between the two types of reactions (Plaetzer *et al.*, 2009).

## 2 Impact of dosimetry to clinical PDT

Explicit PDT dosimetry has been performed in pre-clinical and clinical applications. Among the three components (light, photosensitizer (PS), and oxygen), much work has focused on the measurement of the light fluence and PS concentration. Oxygen transport and consumption during PDT remain important for the modeling of reactive oxygen species (ROS) generation. Currently available methods to measure tissue oxygenation concentration are still in pre-clinical stage. The macroscopic model described in section 3 can be used to calculate the ROS concentration (see Eq. 27) based on explicit dosimetry measurements of light fluence and PS concentration. Current state of art of clinical PDT prescriptions use the product of the drug concentration and light fluence, also called PDT dose.

Pre-clinical mouse studies were performed to compare the correlation of the dosimetric metrics (total light fluence, PDT dose, calculated reacted singlet oxygen) and PDT efficacy (Kim *et al.*, 2015b; Penjweini *et al.*, 2015a; Qiu *et al.*, 2016). Figure 3 shows the comparison between the PDT dose metrics and PDT outcome for BPD-mediated PDT in RIF tumor bearing mice. Cure index, CI = [1 – (tumor growth rate)/(control tumor growth rate)], was used as a measure of tumor control by PDT: CI = 0 no PDT effect; CI = 1 complete PDT cure. It is clear that the correlation is progressively improving from total fluence (Fig. 3 (a)), PDT dose (Fig. 3 (b)), to reacted singlet oxygen, $[^1O_2]_{rx}$ (Fig. 3 (c)), as the grey uncertainty of the correlation reduces with the corresponding goodness of fit R^2 = 0.73, 0.93, and 0.99, respectively.
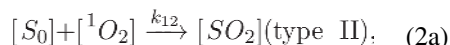
3 Type I and II photosensitized oxidation reactions
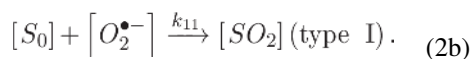
3.1 Photochemical Reactions

The PDT kinetics process was described using rate equations in the literature for microscopic and macroscopic models (Foster *et al.*, 1991; Hu *et al.*, 2005a; Wilkinson and Brummer, 1981; Zhu *et al.*, 2007). The PDT process is started by the absorption of light by the photosensitizer in the ground state, S_0. It is excited into the singlet state, S_1. The S_1 state can spontaneously decay to the ground state with the emission of a photon or heat (Zhu *et al.*, 2007).
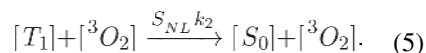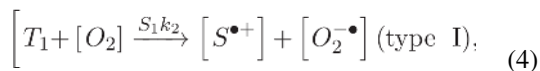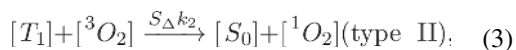
$$[S_0] \underset{k_3}{\overset{k_0}{\longleftrightarrow}} [S_1]. \tag{1}$$
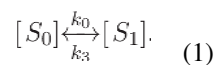
This is a reversible process. The monomolecular absorption rate, k_0 (s^{-1}), is proportional to the light fluence, φ, and the extinction coefficient, ε. The monomolecular decay rate, k_3 (s^{-1}) is the rate from S_1 to S_0. The decay rate due to fluorescence (radiative) is k_{3R} (s^{-1}) and the internal conversion (non-radiative) decay rate is k_{3NR} (s^{-1}), so that $k_3 = k_{3NR} + k_{3R}$ (Sterenborg and van Gemert, 1996). The photosensitizer in its ground state can interact with singlet oxygen and ROS to form a photoproduct [SO_2]. This can be described by the decay rate constant, $k_1 = k_{11} + k_{12}$ (µM^{-1}s^{-1}).

$$[S_0] + [^1O_2] \xrightarrow{k_{12}} [SO_2] (\text{type II}), \quad (2a)$$

and

$$[S_0] + \left[O_2^{\bullet-} \right] \xrightarrow{k_{11}} [SO_2] (\text{type I}). \quad (2b)$$

Similarly, the bimolecular decay rate, k_2 (µM^{1}s^{-1}), describes the rate of interactions by collisions between the triplet state photosensitizer [T_1] and ground state oxygen [$^3O_2$]. A fraction (S_Δ) of the interactions yields singlet oxygen (Eq. 3), while another fraction (S_I) yields the superoxide anion (O$_2$−·) as in (4).

$$[T_1] + [^3O_2] \xrightarrow{S_\Delta k_2} [S_0] + [^1O_2] (\text{type II}), \quad (3)$$

$$\left[T_1 + [O_2] \right] \xrightarrow{S_I k_2} \left[S^{\bullet+} \right] + \left[O_2^{-\bullet} \right] (\text{type I}), \quad (4)$$

$$[T_1] + [^3O_2] \xrightarrow{S_{NL} k_2} [S_0] + [^3O_2]. \quad (5)$$

The last equation shows the fraction ($S_{NL} = 1 - S_\Delta - S_I$) of the interactions between the triplet state photosensitizer and ground state oxygen to produce non-luminescent decay of [T_1] and do not yield singlet oxygen and/or superoxide anion. Physical quenching can also occur where singlet oxygen is converted back to triplet oxygen ($^1O_2 \rightarrow {}^3O_2$). S_I is the fraction of interactions of [T_1] that produce type I reactions.

Triplet decay rate and intersystem crossing of the photosensitizer are described by the monomolecular reaction rates k_4 and k_5 (s^{-1}), respectively. The triplet decay rate includes both the radiative (k_{4R}) and non-radiative (k_{4NR}) decay rate constants.
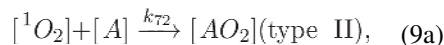
$$[T_1] \xrightarrow{k_4} [S_0]. \quad (6)$$

$$[S_1] \xrightarrow{k_5} [T_1]. \quad (7)$$
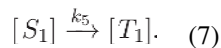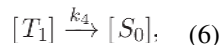
The phosphorescence (or luminescence) of singlet oxygen is described by the monomolecular decay rate k_6 (s^{-1}).

$$[^1O_2] \xrightarrow{k_6} [^3O_2]. \quad (8)$$
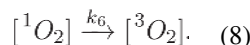
This reaction produces the signature luminescence at 1270 nm. However, there are also non-luminescent reactions of $^1O_2$, such as solvent quenching or physical quenching of $^1O_2$, mentioned above and described later in section 3.1.1 (Wilkinson *et al.*, 1993).

The oxidation of biomolecular acceptors, [A], is described by the decay rate $k_7 = k_{71} + k_{72}$ (s^{-1})

$$[^1O_2] + [A] \xrightarrow{k_{72}} [AO_2](\text{type II}), \quad (9a)$$

and

$$\left[O_2^{-\bullet}\right] + [A] \xrightarrow{k_{71}} [AO_2](\text{type I}). \quad (9b)$$
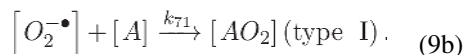
Table 1 summarizes the definition of all rate constants used here along with their conventional names.

3.1.1 Kinetics of Type I Reactions

Type I photooxidation reactions are described by the bimolecular reaction rate $S_I k_2$ (μM^{-1}s^{-1}) with the fraction of triplet interactions that lead to type I reactions (Eq. 4). In a type I reaction, the photosensitizer can undergo electron transfer with oxygen to generate a superoxide anion (O$_2$−·). Superoxide anion, its protonated form HO$_2$· and other radicals such as hydroxyl radicals (HO·) cause cell damage to different degrees (see Fig. 4). Notice that even though all ROSs are generated by the superoxide anion (O$_2$−·) for type I photosensitizer, there are many additional pathways to generate ROS that are not all included in Fig. 4. Details of which can be found elsewhere (Plaetzer *et al.*, 2009). For simplicity, we have lumped these interactions as direct interaction with superoxide anion

(Eq. 9b). Other reactions involve the reaction of the triplet state $[T_1]$ with the molecular substrate directly, described by the reaction rate k_8 ($\mu M^{-1}s^{-1}$):

$$[T]+[A] \xrightarrow{k_8} [TA]. \quad (10)$$
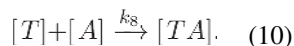
3.1.2 Kinetics of Type II Reactions

Diatomic Oxygen Energy States—The electronic behavior of molecular oxygen results from the arrangement of two electrons in the outer π_g shell (it has a total of 16 electrons since Z = 8 for each O atom) (Kasha, 1985; Greer *et al.*, 2014). Molecular oxygen has an electron configuration in which orbitals are designated as even parity (g = gerade) or odd parity (u = ungerade):

$$(1\sigma_g)^2(2\sigma_u)^2(2\sigma_g)^2(2\sigma_u)^2(3\sigma_g)^2(1\pi_u)^4(1\pi_g)^2$$

where the π_g orbital (formally an open shell) has three possible electron spin arrangements giving rise to three energetically different species: $^3\Sigma_g^-$, $^1\Delta_g$ and $^1\Sigma_g^+$ (Fig. 5). Ground state molecular oxygen ($^3\Sigma_g^-$) is triplet ($I = 1$) and biradical in character; while the two singlet states ($I = 0$) $^1\Delta_g$ and $^1\Sigma_g^+$ both exist on the excited surface. The first excited state ($^1\Delta_g$) is located 22 kcal/mol (0.954 eV, λ = 1270nm) above the ground state with electrons paired in oxygen's degenerate π antibonding orbitals. A valence bond treatment can also be considered: The ionic resonance structures for dioxygen, O^+–O^- and equally contributing O^-–O^+ for $^1\Delta_g$, are unimportant compared to ground-state triplet for O_2 because of the positive charge on oxygen. The second singlet excited state ($^1\Sigma_g^+$) is located 37 kcal/mol (1.6 eV, λ = 755 nm) above the ground state. Quenching of the excited photosensitizers of a high enough energy by the ground state molecular oxygen produces both forms of singlet oxygen (Greer *et al.*, 2014). Because $^1\Delta_g$ oxygen lifetimes are in the microsecond range they can undergo bimolecular reactions; in contrast, the $^1\Sigma_g^+$ oxygen lifetime is short (in the pico- to nanosecond range) (Weldon *et al.*, 1999) and thus chemically unreactive.

Photosensitization routes to $^1\Delta_g$ and $^1\Sigma_g^+$ are of interest. However, the longer lifetime of $^1\Delta_g$ oxygen relates to its chemical reactivity. Chemical reactivity has been generated for $^1\Delta_g$ oxygen with biomolecules, but thus far, no information exists on $^1\Sigma_g^+$ oxygen as a chemically reactive species. Consequently, bimolecular reaction rates for the disappearance of and oxidation by $^1\Delta_g$ oxygen (labeled as $^1O_2$ in this paper) are available.

The reactions of singlet oxygen with substrates can be defined by the rate constants (k_7, k_6). k_7 (also commonly called k_{oa}) is the total reaction rate constant which gives the total rate of disappearance of $^1O_2$ induced by substrate both chemically and physically ($k_{oa} = k_q + \gamma k_r$), where k_q is the physical quenching (quenching of $^1O_2$ due to an interaction with another molecule) rate constant, and k_r is the chemical reaction rate constant of $^1O_2$ which accounts for the rate of formation of oxygenated products. The variable γ relates to the consumption of the product. k_6 (also commonly called k_d) is rate constant for natural decay of $^1O_2$ back

to $^3O_2$ (also called solvent quenching). For example, amines efficiently deactivate $^1O_2$ back to $^3O_2$ by charge-transfer quenching and carotenoids efficiently deactivate $^1O_2$ back to $^3O_2$ by energy-transfer quenching (Musbat *et al.*, 2013; Catalan *et al.*, 2003; Rodgers and Lee, 1984).

In vivo photochemical reactions of singlet oxygen—Over the past three decades, the reactivity of $^1O_2$ has been explored. Singlet oxygen reacts with compounds and biological material to give oxygenated products, such as endoperoxides from [2 + 4] cycloadditions, dioxetanes from [2 + 2] cycloadditions, oxides from heteroatom oxidations, hydroperoxides from "ene" reactions and tandem $^1O_2$ reactions (Zamadar and Greer, 2010; Turro *et al.*, 2010). Reactions of singlet oxygen with small biomolecules have been carried out. For example, mechanisms have been studied such as the photooxidation of bilirubin and guanosine and ascorbic acid derivatives. Examples of $^1O_2$ reactions in the organic chemistry that are models of biological reactions are listed in Appendix A, where the rate constants of individual reactions provide some insight to an overall photooxidative outcome in a biological system.

Chemical trapping of $^1O_2$ is known in solution with biomolecules. The reactivity of $^1O_2$ with biomolecules (e.g., membranes and lipids), amino acids (e.g., His, Trp, and Met), and nucleic acids (e.g., guanosine) as model systems to help in understanding the mechanism of toxiciy in PDT (Cadet *et al.*, 2006; Girotti, 2001; Itri *et al.*, 2014; McDonagh, 2001; Kanofsky, 1989). Reaction of $^1O_2$ with methionine is an example of heteroatom oxidation in proteins (Fig. 6). For methionine, two moles of methionine sulfoxide form per mole of $^1O_2$ in the reaction ($\gamma = 2$). Certain biomolecules such as amines and carotenes can serve as protection against singlet oxygenation in converting $^1O_2$ to $^3O_2$ by physical quenching (as was mentioned above).

3.2 Explicit Model of Type I and II Photodynamic Interactions

For both type I and II primary photochemical reactions, as explained in section 3.1, a set of coupled differential equations can be used to describe the PDT process (Finlay *et al.*, 2001; Wang *et al.*, 2010; Wang *et al.*, 2007; Weston and Patterson, 2011; Zhu *et al.*, 2007):

$$\frac{d[S_0]}{dt} = -k_0[S_0] - k_{12}[^1O_2]([S_0]+\delta) - k_{11}[O_2^{-\bullet}]([S_0]+\delta) + k_2[T_1][^3O_2] + k_3[S_1] + k_4[T_1], \quad (11)$$

$$\frac{d[S_1]}{dt} = -(k_3+k_5)[S_1] + k_0[S_0], \quad (12)$$

$$\frac{d[T_1]}{dt} = -k_2[T_1][^3O_2] - k_4[T_1] + k_5[S_1] - k_8[T_1][A], \quad (13)$$

$$\frac{d[^3O_2]}{dt} = -S_\Delta k_2[T_1][^3O_2] - S_1 k_2[T_1][^3O_2] + k_6[^1O_2] + \Gamma, \tag{14}$$

$$\frac{d[^1O_2]}{dt} = -k_{12}[^1O_2]([S_0]+\delta) + S_\Delta k_2[T_1][^3O_2] - k_6[^1O_2] - k_{72}[A][^1O_2], \tag{15}$$

$$\frac{d[O_2^{-\bullet}]}{dt} = -k_{11}[O_2^{-\bullet}]([S_0]+\delta) + S_1 k_2[T_1][^3O_2] - k_{71}[A][O_2^{-\bullet}], \tag{16}$$

$$\frac{d[A]}{dt} = -k_{72}[A][^1O_2] - k_{71}[A][O_2^{-\bullet}] - k_8[T_1][A]. \tag{17}$$

These equations are based on the kinetic equations of the photochemical reactions using their rate constants, $k_0, \ldots, k_8$ (see their definitions in table 1). Here, $[S_0]$, $[S_1]$, and $[T_1]$ are the ground, first excited singlet, and triplet photosensitizer concentrations respectively. $[^3O_2]$ and $[^1O2]$ are the ground triplet and excited singlet state oxygen concentrations. $[O_2-\cdot]$ is the concentration of superoxide anion and represents the amounts of ROS in a type I mechanism. Γ and $[A]$ are the oxygen supply rate and the concentration of ($^1O_2$ and ROS) acceptors excluding the photosensitizer molecule. Depending on the methods used to determine the oxygen supply rate in (14), the model is divided into microscopic and macroscopic models. In the microscopic model, oxygen diffusion into capillaries, from capillaries into tissue, and diffusion within tissue is used to calculate the Γ term (Wang *et al.*, 2007). For more details on the microscopic singlet oxygen model, see Appendix B. Based on the kinetic equations of the photochemical reactions, the oxygen supply term in a macroscopic theory can be expressed as: (Hu *et al.*, 2005b; Zhu *et al.*, 2007; Wang *et al.*, 2010; Zhu *et al.*, 2015c)

$$\Gamma = g\left(1 - \frac{[^3O_2]}{[^3O_2]_0}\right), \tag{18}$$

where g is the macroscopic maximum oxygen supply rate and $[^3O_2]_0$ is the initial tissue oxygen concentration. In the macroscopic model, the Γ term is assumed to be uniformly distributed everywhere without consideration of oxygen diffusion through the vasculature. The functional form of equation (18) was validated using forward calculations with standard vascular parameters (Zhu *et al.*, 2015c). Since the spatial scale of light transport is much larger than the spatial scale of oxygen diffusion (~1 mm versus ~65 μm), the light fluence

rate was also set to be a constant within the vasculature model (Zhu and Liu, 2013; Zhu *et al.*, 2015c). This term ensures that the oxygen level does not exceed the initial value.

Due to the short lifetime and diffusion distance of $^1O_2$ in biological media, the term for the photobleaching kinetics for ground state photosensitizer undergoing $^1O_2$-mediated bleaching has the low concentration correction constant, δ (Finlay et al., 2004; Moan and Berg, 1991). $^1O_2$ is generated at the site of the parent photosensitizer molecule. Due to the short diffusion distance (10-100 nm (Moan and Berg, 1991; Niedre *et al*, 2002)), it has a higher probability of reacting with the parent photosensitizer molecule than with adjacent photosensitizer molecules. For low photosensitizer concentrations, the rate of photobleaching depends only on the rate of $^1O_2$ generation because the volume through which each $^1O_2$ can diffuse before reacting will contain exactly one photosensitizer molecule, independent of the total photosensitizer concentration. In other words, δ is the concentration of $[S_0]$ where intermolecular distance is equal to the $^1O_2$ diffusion distance (Dysart *et al.*, 2005). The value of this critical low photosensitizer concentration is estimated to be between 3 and 3000 μM (Dysart and Patterson, 2005). δ can be expressed as

$$\delta = \frac{1}{d^3 N_A}. \quad (19)$$

Here, d is the diffusion distance of $^1O_2$ in the environment of interest, which can be related to τ_Δ by $d = (6D\tau_\Delta)^{1/2}$, where D is the diffusion coefficient for $^1O_2$ and N_A is Avogadro's number (Dysart *et al.*, 2005).

If one only cares about the dynamic process of PDT in the time scale of a few seconds to hours, then the time derivative in the right hand sides of equations (12), (13), and (15) can be set to zero because these processes are known to be very fast (~ μs or less). They can then be simplified to:

$$[S_1] = \tau_f \frac{\varepsilon}{h\nu} \phi [S_0], \quad (20)$$

$$[T_1] = \frac{\Phi_t}{[^3O_2] + \beta} \frac{1}{k_2} \frac{\varepsilon}{h\nu} \phi [S_0]. \quad (21)$$

$$[^1O_2] = \xi_{II} \tau_\Delta \frac{[^3O_2]}{[^3O_2] + \beta} \phi [S_0], \quad (22)$$

$$[O_2^{-\bullet}] = \xi_I \tau_s \frac{[^3O_2]}{[^3O_2]+\beta} \phi[S_0]. \tag{23}$$

$$\frac{d[S_0]}{dt} = -\frac{[^3O_2]}{[^3O_2]+\beta} \xi\sigma([S_0]+\delta)\phi[S_0] - \eta\frac{1}{[^3O_2]+\beta}\phi[S_0], \tag{24}$$

$$\frac{d[^3O_2]}{dt} = -\frac{[^3O_2]}{[^3O_2]+\beta}\phi[S_0](\xi_{II}(\sigma_{II}([S_0]+\delta)+k_{72}[A]\tau_\Delta)+\xi_I)+g\left(1-\frac{[^3O_2]}{[^3O_2](t=0)}\right), \tag{25}$$

$$\frac{d[A]}{dt} = -\frac{[^3O_2]}{[^3O_2]+\beta}\phi[S_0](\xi_{II}k_{72}[A]\tau_\Delta+\xi_I) - \eta\frac{1}{[^3O_2]+\beta}\phi[S_0]. \tag{26}$$

All of the parameters (ξ, ξ_I, ξ_{II}, σ, σ_I, σ_{II}, τ_f, τ_Δ, τ_s) have been defined in Table 2. *In-vivo*, ($\xi_{II}(\sigma_{II}([S_0]+\delta)+k_{72}[A]\tau_\Delta)+\xi_I$) in Eq. 25 and ($\xi_{II}k_{72}[A]\tau_\Delta+\xi_I$) in Eq. 26 can be replaced with ($\xi = \xi_{II} + \xi_I$) since $k_{72}[A]\tau_\Delta \approx 1$ and $\sigma_{II}([S_0]+\delta) \ll 1$. Utilizing Eq. 26 above, the amount of biological acceptor that has reacted with a reactive oxygen species ($[ROS]_{rx}$) can be defined by the following

$$\frac{d[ROS]_{rx}}{dt} = -f\xi\frac{[^3O_2]}{[^3O_2]+\beta}[S_0]\phi - \eta\frac{1}{[^3O_2]+\beta}[S_0]\phi. \tag{27}$$

where *f* is the fraction of ROS interacting with [*A*]. Here, the first term relates to the fraction of acceptors that reacted due to reactive oxygen species (ROS)-mediated reactions, and the second term relates to the fraction that reacts under hypoxic conditions or any other non-oxygen-mediated reactions, such as triplet interactions. In cases where type II reactions dominate ($S_\Delta \gg S_I$ and $\eta = 0$), the reacted singlet oxygen ($[^1O_2]_{rx}$) can be defined by

$$\frac{d[^1O_2]_{rx}}{dt} = -f\left(\xi\frac{\phi[S_0][^3O_2]}{[^3O_2]+\beta}\right). \tag{28}$$

The required photochemical parameters can be reduced from 11 (δ, g, k_0, …, k_8) to 6 (δ, β, ξ, σ, η, g), with some of the latter expressed as ratios of the former, if one is not interested in modeling [S_1], [T_1], [$^1O_2$], and [$O_2^{-\cdot}$]. The definitions for the photochemical parameters,

ξ, β, η, δ, and σ, are shown in table 2, along with their relationships to the reaction rate constants.

The specific oxygen consumption rate, ξ, is the PDT oxygen consumption rate per light fluence rate and photosensitizer concentration under the condition that there is an infinite $^3O_2$ supply. σ, the specific photobleaching ratio, is the probability ratio of a ROS (including $^1O_2$ molecule) to react with ground state photosensitizer compared to the ROS (including $^1O_2$ molecule) reacting with a cellular target *[A]*. Notice that ξ and σ contains PDT photodynamic interaction from both type I and type II and are not separated. β represents the ratio of the monomolecular decay rate of the triplet state photosensitizer to the bimolecular rate of the triplet photosensitizer quenching by $^3O_2$ (Wang *et al.*, 2010) and is called the oxygen quenching threshold concentration (Zhu *et al.*, 2015a). η is the hypoxic consumption rate due to photobleaching reactions.

Table 2 also provides the definition of several other important photochemical parameters for a specific photosensitizer. Fluorescence quantum yield (Φ_f) of a compound is defined as the fraction of molecules that emit a photon after direct excitation (Demas and Crosby, 1971). The triplet quantum yield (Φ_t) describes the crossover efficiency for photosensitizers to go from the singlet state to the triplet state via intersystem crossing (Bensasson *et al.*, 1972). Similarly, the singlet oxygen quantum yield (Φ_Δ) is given as the efficiency to produce singlet oxygen from the triplet state of a photosensitizer (Wilkinson *et al.*, 1993). We have introduced superoxide anion quantum yield (Φ_{ROS}) as the efficiency of producing superoxide anion from the triplet state of a photosensitizer. In addition to the quantum yields, the fluorescence lifetime (τ_f), triplet lifetime (τ_t), and singlet oxygen lifetime (τ_Δ) represent mean lifetime of each state (i.e. of the fluorescent state, the triplet state, and of singlet oxygen) (Strickler and Berg, 1962). e is the extinction coefficient (cm^{-1}μM^{-1}) defined as the absorption coefficient of the photosensitizer per concentration.

3.3. Relationship between rate parameters and the photochemical parameters

The rate constants for each of the reactions described previously can be determined by knowing some of the basic photochemical parameters mentioned before including the singlet oxygen lifetime (τ_Δ), the fluorescence lifetime (τ_f), the triplet lifetime (τ_t), and the triplet quantum yield (Φ_t), all of which are measureable quantities with existing technologies, which is described in section 4.

The photon absorption rate of the photosensitizer is given by knowing the extinction coefficient (ε) of the photosensitizer, the fluence rate ($\phi = 100$ mW/cm), Planck's constant (h), and the frequency of light used for treatment (ν).

$$k_0 = \frac{\varepsilon \dot{\phi}}{h\nu}. \quad (29)$$

The reaction rates involving $^1O_2$ (k_1, k_6, k_7) can be determined by measuring the singlet oxygen lifetime. The relationship between τ_Δ and the rate constants is the following:

$$\tau_\Delta^{-1} = k_1 \left([S_0] + \delta \right) + k_6 + k_7 [A]. \quad (30)$$

By varying the concentration of $[S_0]$ in water in the absence of any molecular singlet oxygen acceptors ($[A] = 0$), the plot of τ_Δ^{-1} versus $[S_0]$ will yield a slope which will be k_1 with a low concentration correction (δ) (Dysart and Patterson, 2005, 2006). Furthermore the extrapolation to $[S_0] = 0$ will yield the value of k_6, provided that the values of δ and k_1 are known. Adding known concentrations of acceptors will allow for extrapolation of the value k_7. The value of δ can be found by investigating photobleaching kinetics and the steady-state singlet oxygen concentration approximation (Dysart *et al.*, 2005).

Triplet quantum yield (Φ_t) and fluorescence decay time (τ_f) can be used to calculate k_3 and k_5 with the following equations (Sterenborg and van Gemert, 1996)

$$\tau_f = \frac{1}{k_3 + k_5}; \quad (31)$$

$$k_3 = \frac{1 - \Phi}{\tau_f}; \quad (32)$$

$$k_5 = \frac{\Phi}{1 - \Phi_t} \cdot k_3 = \frac{\Phi_t}{\tau_f}. \quad (33)$$

Rate reactions involving the triplet state photosensitizer (k_2, k_4, k_8), are related to the triplet state lifetime by

$$\tau_t^{-1} = k_4 + k_2 [^3O_2] + k_8 [A]. \quad (34)$$

Measurement of the ground state oxygen in a phantom will enable extrapolation of k_2 and k_4 in a linear fit of τ_t^{-1} versus $[^3O_2]$ with the slope gives k_2 and extrapolation to $[^3O_2] = 0$ gives $k_4 + k_8[A]$. The oxygen quenching threshold concentration β ($= (k_4 + k_8[A])/k_2$) in the macroscopic model can be calculated with the ratio of the two. k_8 can be determined as the slope between τ_t^{-1} and $[A]$. All other photophysical parameters (ξ, σ, η) can be determined using the rate, k_i and the expression in Table 2.

The quantum yield for generation of singlet oxygen (Φ_Δ) and superoxide anion (Φ_{ROS}) are important quantities in determining the concentrations of the cytotoxic oxygen species. Both are related to the photosensitizer triplet quantum yield by

$$\Phi_\Delta = S_\Delta \Phi_t. \quad (35)$$

$$\Phi_{ROS} = S_I \Phi_t. \quad (36)$$

4. Experimental methods to determine the rate parameters

The advent of spectroscopic techniques to measure rate constants of photosensitization and oxygenation has opened the way to the determination of their photochemical and photophysical parameters. This section describes a sampling of methods to determine experimental rate parameters and other key photochemical factors. The scope of this review is focused mainly on photochemical parameters *in-vivo*. At present, this is only achievable through indirect methods (section 4.2) – namely extrapolation of the parameters in table 2 by applying the macroscopic model directly in *in-vivo* systems. Most, if not all, of the direct methods to determine reaction rates are limited to *in-vitro* systems or in phantoms. We will point out the potential for direct methods to *in-vivo* system whenever possible. In addition, section 5 will point out the reaction rates that are inferred from *in-vitro* measurements and are expected to remain the same *in-vivo*.

4.1 Direct Methods

4.1.1 Absorption Spectroscopy—Absorption spectroscopy refers to a technique that measures the absorption of radiation by a sample. By using a spectrophotometer and a white light source, the extinction coefficient (ε; units cm^{-1}μm^{-1}) of a photosensitizer can be determined by the Beer-Lambert law (Fuwa and Valle, 1963; Walsh, 1955):

$$A = -\ln\frac{I}{I_0} = \varepsilon l c, \quad (37)$$

where I is the output light intensity, I_0 is the input light intensity, l is the path length of the measured sample, and c is the concentration of the sample (in μM). Typically, absorbance, A, is defined for $l = 1$ cm). Notice our definition of extinction coefficient is $\log_e$ based rather than $\log_{10}$ based, the later is often the case in the chemistry literature and cause **s** to be decreased by a factor of 2.30 (ln10). Using Eq. (27), the value of k_0 can easily be determined from the measured ε and knowing the measured wavelength, λ, of the light ($h\nu = hc/\lambda$).

Transient Absorption Spectroscopy: Transient absorption spectroscopy is an extension of absorption spectroscopy. Also called pump-probe spectroscopy, the absorbance of a sample is measured as a function of time after excitation by a flash of light, usually a pulsed laser, mainly to determine the triplet lifetime of the sensitizer, $[T_1]$ (Aveline *et al.*, 1998). This technique can be used to measure the singlet oxygen quantum yield (Φ_Δ) for a photosensitizer utilizing another chemical with known singlet oxygen quantum yields. (Krieg and Redmond, 1993; Krieg *et al.*, 1993a).

4.1.2 Fluorescence Spectroscopy—Photosensitizer fluorescence can be used to determine the concentration ($[S_0]$) of photosensitizer present both *in-vivo* and *in-vitro* (Konig *et al.*, 1993; Robinson *et al.*, 1998). However, fluorescence signal *in-vivo* is affected by the tissue optical properties of scattering and absorption. The reduction of the fluorescence signal due to absorption can be accounted for by incorporating an empirical correction factor based on tissue optical properties (Finlay *et al.*, 2006). Many commonly used photosensitizers produce unique fluorescence spectra when excited at a certain wavelength. Figure 7 shows an example of three photosensitizers (BPD, HPPH, and Photofrin) and their fluorescence spectra excited at 405 nm. Such emission spectra, corrected for instrument response and tissue optical properties, can be analyzed as a linear combination of fluorescence basis spectra using a singular value decomposition (SVD) fitting algorithm (Finlay *et al.*, 2001). Fluorescence spectra from phantoms with known photosensitizer concentrations can be used to determine the correction factor for fluorescence due to tissue optical properties as well as the absolute value of $[S_o]$ in an *in-vivo* environment (Finlay *et al.*, 2006).

Fluorescence Lifetime Spectroscopy and Imaging (FLI): Time-resolved fluorescence decay measurements can be used to study details about the structure and dynamics of macromolecules. These measurements are commonly performed with microsecond to picosecond laser sources with high-speed photodetectors (Lakowicz *et al.*, 1992).

The fluorescence lifetime, τ_f, of photosensitizers can be determined from time-gated spectra along with single photon counting, using a picosecond to microsecond pulsed diode laser for fluorescence excitation. Specific wavelength ranges can be selected to plot the fluorescence exponential decay curve ($e^{-(k_3+k_5)t}$) to yield the decay constant (k_3+k_5), which can be used to calculate $\tau_f = 1/(k_3+k_5)$ (Kress *et al.*, 2003).

Laser-induced Optoacoustic Calorimetry (LIOAC): Triplet quantum yields, Φ_t, can be obtained by LIOAC and oxygen fluorescence quenching. After a laser pulsed excitation at the absorption wavelength (e.g., 532 nm) of the photosensitizer, radiationless relaxation processes of the intermediate states (e.g., S1, T1, …) causes rapid deposition of heat in the sample, giving rise to acoustic waves, the magnitude of which is directly proportional to the heat evolved and can be detected by a piezoelectric transducer (Aveline *et al.*, 1994). The absorbed energy deposited as heat in the sample within the detection window, αE_{abs} can be used to calculate the fluorescence and triplet quantum yield using (Aveline *et al.*, 1994):

$$(1 - \alpha)E_{abs} = \Phi_f E_s + \Phi_t E_t, \quad (38)$$

where E_s and E_t are the singlet state and triplet state energy gaps to the ground state, respectively. Experimentally, α is determined by comparing the calorimetric energy balance for the sample in question to an ideal reference system, which has a known $\alpha = 1$ (Aveline *et al.*, 1994).

4.1.3 Phosphorescence Spectroscopy—Phosphorescence is similar to fluorescence in that absorbed energy by a substance is released in the form of light. However, phosphorescence occurs on a longer time scale than fluorescence. Besides the decays from monomol $^1O_2$ to $^3O_2 + h\nu$ at 1270 nm (22 kcal/mol), dimol singlet oxygen molecules $(2\ ^1O_2)$ can also decay to 2 moles $^3O_2 + h\nu$ at 634 nm (44 kcal/mol) and 701 nm (Khan and Kasha, 1963, 1964, 1970; Arnold *et al.*, 1964; S. *et al.*, 1965). The latter (634 nm and/or 701 nm) is readily observed in the gas phase but is often not used due to other optical signals at these wavelengths. The detection of $^1O_2$ luminescence at 1270 nm is still difficult because of the short lifetime of $^1O_2$.

Singlet Oxygen Luminescence (SOL) Detection (or Laser flash photolysis): SOLD (or laser flash photolysis) is a standard technique for identification of short-lived, excited states of photosensitizers and characterization of their reactions (Hurst *et al.*, 1982; Khan and Kasha, 1979; Krasnovskii, 1976). It is a popular and precise technique used to directly measure k_6 and k_7, where the photosensitizer solution of the substrate is saturated with O_2 and irradiated with laser at a specific absorption wavelength. The resulting phosphorescence of $^1O_2$ at 1270 nm as a function of time is measured with a time-correlated detector (Kanofsky, 1990). With the TCSPC module, phosphorescence decay characteristics can be measured with a time resolution of $\leq$100 ps and a spatial resolution in the subcellular region. With a high pulse repetition rate (40 MHz), the total acquisition time is short (less than 1 s) for each fluorescence decay curve (Kress *et al.*, 2003). Production of $^1O_2$ by laser excitation occurs in less than 2 μs, its decay is approximated by equation (40) (derived from equation (15)) and a first-order exponential decay of $^1O_2$ is given in equation (41). A Stern-Volmer plot of concentration of substrate *[A]* versus $1/\tau_\Delta$ (where τ_Δ is the experimentally measured singlet oxygen lifetime), gives a straight line with the slope equal to k_7 and the y-intercept equal to k_6:

$$-\frac{d[^1O_2]}{dt} = \frac{1}{\tau_\Delta}[^1O_2] \quad (39)$$

$$[^1O_2] = [^1O_2]_0 e^{-t/\tau_\Delta} \quad (40)$$

$$\tau_\Delta^{-1} = k_6 + k_7[A] = k_d + (k_q + \gamma k_r)[A] \quad (41)$$

The rate constants for oxidized product formation, k_r are obtained by a competition technique reported by Higgins *et al.* (Higgins *et al.*, 1968) where the substrate solution containing photosensitizer and an alkene for comparative trapping to deduce the contribution from physical quenching k_q, can be obtained by difference using Eq. (41) (Celaje *et al.*, 2011; Clennan *et al.*, 1995). The variable γ in Eq. (41) is a function of the product chemical composition (see figure 5, $\gamma = 2$). Unlike unsaturated compounds such as alkenes, amines

and polyenes are effective singlet oxygen physical quenchers and protect against photooxygenation (Wessels and Rodgers, 1995).

Singlet oxygen quantum yields (Φ_Δ) can be determined from the phosphorescence intensity extrapolated back to zero time. These values can be recorded as a function of laser energy and of the solution absorbance for the sample and reference photosensitizers. Linear plots of the energy at each absorbance can be plotted (with the absorption factor) to produce slopes equivalent to the quantum yield (Marti *et al.*, 2000).

Measurement of this near-infrared (NIR) luminescence of singlet oxygen in biological environments is difficult due to the reduced $^1O_2$ lifetime (which is much less than the triplet-state lifetime). However, this can be achieved using a NIR-sensitive photomultiplier tube. Time-resolved analysis shows that $^1O_2$ lifetime is reduced ($\tau_\Delta = 0.03$-0.18 μs) *in-vivo* compared to lifetime *in-vitro* ($\tau_\Delta = 3.0 \pm 0.3$ μs). This may be due to the protein binding to $^1O_2$ in cellular environments (Niedre *et al.*, 2002). The photomultiplier tube must be sufficiently fast (with a rise time of ~ 3 ns) for phosphorescence single-photon counting, and it must have a broad, flat spectral response that enables spectral resolution of the $^1O_2$ signal (Jarvi *et al.*, 2006).

The shorter lifetime has been attributed to the rapid quenching of $^1O_2$ by biomolecules, combined with a lack of adequately sensitive detectors at near-infrared wavelengths, since the luminescence emission is proportional to the lifetime.

When exchanging the H_2O solvent for D_2O, the lifetime of singlet oxygen increases by 20-fold. The τ_Δ in D_2O is 69 μs at 20°C and in H_2O 3.5 μs at 20°C (Jensen *et al.*, 2010; Ogilby and Foote, 1983; Wilkinson *et al.*, 1993).

The triplet-state lifetime is highly dependent on the molecular oxygen concentration according to a Stern-Volmer relationship

$$\tau_t^{-1} = k_{4R} + k_{4NR} + k_2[^3O_2] = k_4 + k_2[^3O_2] \quad (42)$$

where k_{4R} and k_{4NR} are the radiative and nonradiative photosensitizer triplet state decay rate constants. The changes in triplet state lifetime (τ_t) can be used to determine changes in $[^3O_2]$, given k_2 and k_4 is known. In biological systems, $\tau_t \gg \tau_\Delta$ so that the exponential decay of the singlet oxygen luminescence curves is governed by τ_t (Jarvi *et al.*, 2006; Poole *et al.*, 2004; Shonat and Kight, 2003).

Most singlet oxygen luminescence dosimetry (SOLD) studies have been done on microspheres of cells. Detection of SOL from a murine tumor using Photofrin and ATX-S10NA(a) has been reported (Hirano *et al.*, 2002). The full luminescence spectrum can be measured by placing a monochromator in front of the detector.

The great impact of SOLD techniques comes with reports that show detection of $^1O_2$ in complex biological systems directly. The integrated detected $^1O_2$ luminescence counts is

proportional to the total amount of $^1O_2$ created in the target during PDT and thus is predictive of PDT response (Jarvi *et al.*, 2006). Ultimately it is the cumulative $^1O_2$ dose that determines the biological effect. Furthermore, changes in the effective PDT dose due to oxygen depletion or due to photosensitizer photobleaching can be evaluated with time-resolved SOL measurements.

4.2 Indirect Methods

Singlet oxygen explicit dosimetry (SOED) methods have been developed to calculate the reacted singlet oxygen, $^1[O_2]_{rx}$, *in-vivo* and *in-vitro* for type II photosensitizers. The main cytotoxic agent in type II PDT has been attributed to $^1O_2$ (Weishaupt *et al.*, 1976). PDT efficacy can be correlated to the calculated $^1[O_2]_{rx}$, thus making SOED an effective method of dosimetry for *in-vivo* studies as well as in clinical settings. The methodology for SOED for type II photosensitizer can be expanded for ROS involving type I photosensitizers, even though it has not been used in existing studies. However, the parameters obtained should include photodynamic action from both type I and type II even though singlet oxygen is predominant for the type II photosensitizers studied.

4.2.1 Singlet Oxygen Explicit Dosimetry in-vitro and in Phantoms—Singlet oxygen explicit dosimetry methods have been used *in-vitro* to determine photochemical parameters in Table 2 (β, δ, ξ, and σ) (Dysart and Patterson, 2006; Foster *et al.*, 1993; Foster *et al.*, 1991; Georgakoudi *et al.*, 1997; Nichols and Foster, 1994; Patterson *et al.*, 1990). Spheroids of cell have been used to model PDT-induced oxygen depletion using equations very similar to those of section 3.2. Cell suspensions in cuvettes have been irradiated to investigate PDT *in-vitro* and light dose dependent effects (Sporn and Foster, 1992). Cell survival assays are used as an endpoint to assess fluorescence-based singlet oxygen dose metrics (Dysart and Patterson, 2006). In phantoms, singlet oxygen can be trapped by various compounds and thus detected indirectly. Most common compounds for $^1O_2$ are SOSG and MNR as described in section 4.3.

Spheroid cell survival assays have been used to determine the threshold dose of singlet oxygen for necrosis as well as photochemical parameters (β, δ, ξ and σ) (Foster *et al.*, 1993; Georgakoudi *et al.*, 1997). Monolayers of cell cultures are initiated into spheroids ~500μm in diameter. Treated spheroids are dissociated and the fraction of cells that survive treatment is determined by a colony formation assay (Foster *et al.*, 1993; Georgakoudi *et al.*, 1997). An expression that relates the experimentally determined spheroid cell surviving fraction to the total rate of oxygen consumption (the sum of both metabolic oxygen consumption rate, which is assumed to be unaffected by PDT, and the oxygen consumption rate due to PDT processes) is used to determine a coefficient of PDT-induced oxygen consumption. Furthermore, a threshold dose of $^1O_2$ can be determined for cell spheroids, where once this dose has been delivered to the cells within the spheroid shell and $^3O_2$ has been depleted, continued irradiation at the same fluence rate will not result in significant additional cell killing (Foster *et al.*, 1993). Measurements of $^3O_2$ depletion and a knowledge of $^3O_2$ diffusion in cells and consumption due to PDT can be used to describe $^3O_2$ transport in a cell spheroid system. This can further be used to calculate the amount and distribution of $^1O_2$ molecules in a multicell-spheroid model during PDT (Nichols and Foster, 1994).

Oxygen consumption and photobleaching studies with spheroids cells have been used to determine the probability of $^1O_2$ reaction with ground state photosensitizer, σ ($k_1/k_7[A]$) as well as the ratio of k_4/k_2 (β). Using measurements from oxygen microelectrodes, the following equation for oxygen consumption was fit to determine σ (Georgakoudi and Foster, 1998; Georgakoudi et al., 1997)

$$\frac{d[^3O_2]}{dt}(t) = \xi [S_0]_0 \phi \left(\frac{[^3O_2](t)}{[^3O_2](t)+\beta} \right) \exp \left(-\sigma \int_0^t \frac{d[^3O_2]}{dt}(t')dt' \right) \tag{43}$$

The left hand side of Eq. (43) is the rate of photodynamic oxygen consumption and $\xi[S_0]_0$ is the maximum or initial rate of photodynamic oxygen consumption occurring in two phases for the experiment of oxygen consumption during PDT, which is a function of the incident fluence. In this spheroid model, the oxygen perfusion rate (g) present in Eq. (25) is set to 0 since no vasculature is present. Georgakoudi et al. found that σ is 90 ± 15.9 M^{-1} for ALA-induced PpIX photobleaching and 76 ± 12 M^{-1} for Photofrin (Georgakoudi et al., 1997) assuming a uniform distribution of photosensitizer. Spheroid cells and oxygen microelectrode measurements have also been used to investigate β. Mitra et al. have found that β is 8.7 ± 2.9 μM for mTHPC-mediated PDT and σ is 29.7 ± 4.6 M^{-1} (Mitra and Foster, 2005). Reanalysis of Photofrin data with the observation of Photofrin's nonuniform distribution yielded values of $\beta = 12.1 \pm 3.4$ μM and $\sigma = 56.5 \pm 8.6$ M^{-1} (Mitra and Foster, 2005), which is not remarkably different from $\beta = 11.9 \pm 2.2$ μM as determined with an assumed uniform distribution of Photofrin (Georgakoudi et al., 1997). The threshold dose of $^1O_2$ in spheroid cells using Photofrin-mediated PDT was found to be 11.9 ± 3.5 mM (Mitra and Foster, 2005).

4.2.2 Singlet Oxygen Explicit Dosimetry in-vivo—For SOED, it is critical to know the four photochemical parameters, (ξ, σ, δ, and g), and the singlet oxygen threshold dose, $[^1O_2]_{rx,sh}$. These parameters can be determined by performing PDT on a mouse model (Kim et al., 2015a; Kim et al., 2014a; Kim et al., 2015b; Liang et al., 2012; Liu et al., 2014; Liu et al., 2013; McMillan et al., 2013; Penjweini et al., 2015a; Wang et al., 2010; Zhu et al., 2007; Zhu et al., 2015a; Zhu and Liu, 2013; Zhu et al., 2014). Tumors are grown on mice and after injection with photosensitizer, treatment is delivered interstitially using a cylindrically diffusing fiber inserted inside the tumor. Partial treatment of the tumor is performed using various light doses and fluence rates. After treatment, the tumors are sectioned perpendicular to the linear treatment and stained with hematoxylin and eosin (H & E) to assess the necrotic area. Necrotic area is then used to calculate necrosis radius ($A = \pi r^2$, where A is the area and r is the necrosis radius). PDT-induced necrosis is determined by subtracting the radius of necrosis from control mice with no PDT treatment. Necrosis radius is then used with the spatially- and temporally-resolved calculated $^1[O_2]_{rx}$ profile using the macroscopic model equations from section 3.2. Experimentally obtained data is used for the model equations. Light fluence distribution inside the tumor is calculated by measuring the absorption and scattering optical properties (μ_a and μ_s') (Zhu et al., 2005). Photosensitizer concentration inside the tumor is determined using fluorescence spectra that are corrected for optical

property effect (Finlay *et al.*, 2001). The correction factor is determined prior to experimentation in phantom studies with known photosensitizer concentrations and varying optical properties (Kim *et al.*, 2014a; Kim *et al.*, 2015b).

The model parameters are then varied globally so that the $[^1O_2]_{rx}$ for each mouse at the necrosis radius is close to the "apparent $[^1O_2]_{rx,sh}$." This quantity is then the singlet oxygen threshold dose. An initial guess for these model parameters must be provided for the fitting routine. Initial *in-vivo* model parameters have been published previously. (Kim *et al.*, 2015a; Kim *et al.*, 2014a; Kim *et al.*, 2015b; Liang *et al.*, 2012; Liu *et al.*, 2014; Liu *et al.*, 2013; McMillan *et al.*, 2013; Penjweini *et al.*, 2015a; Wang *et al.*, 2010; Zhu *et al.*, 2007; Zhu *et al.*, 2015a; Zhu and Liu, 2013; Zhu *et al.*, 2014) Threshold singlet oxygen doses ($[^1O_2]_{x,sh}$) *in-vivo* using mouse models were fitted to be 0.56 ± 26 mM, 0.72 ± 21 mM, and 0.60 ± 18 mM for Photofrin, BPD, and HPPH respectively (Kim *et al.*, 2015a; Kim *et al.*, 2014a; Kim *et al.*, 2015b; Liu *et al.*, 2014; McMillan *et al.*, 2013; Wang *et al.*, 2010; Zhu *et al.*, 2015a). The other parameters are summarized in Table 5.

4.3 Other Methods

In addition to the experimental methods mentioned in this section, there are other techniques that can be used to investigate the presence of the cytotoxic species. These methods have been mostly used *in vitro*; however, some may be applicable in *in vivo* systems as well. These methods involve fluorescent markers and analytical methods.

Several methods are developed to detect the presence of singlet oxygen and/or HO·. Singlet oxygen can be detected from dioxetanes from [2 + 2] cycloadditions, endoperoxides from [2 + 4] cycloadditions, and allylic hydroperoxides from 'ene' reactions (Clennan and Foote, 1992; Aubry *et al.*, 2003). Simple alkenes often take up 1 equivalent of $^1O_2$. Tandem $^1O_2$ reactions can take place in polyunsaturated compound, there are also instances where bisperoxides rearrange to spiro compounds. Peroxides can also be generated through type I reaction that do not involve singlet oxygen, for example, there are electron transfer photooxidation reactions with 9-mesityl-10-methylacridinium ion (Ohkubo *et al.*, 2005; Kotani *et al.*, 2004). It may be noted that ene-derived hydroperoxides and cycloaddition-derived endoperoxides have a toxicity of their own that is separate of singlet oxygen's toxicity. (Chakraborty *et al.*, 2009; Ouedraogo and Redmond, 2003)

Aromatic compounds such as 9,10-disubstituted anthracenes can trap $^1O_2$ and be detected by UV-vis spectroscopy (Ragas *et al.*, 2009; Kim *et al.*, 2014b; Pedersen *et al.*, 2014). Another trapping reaction is 9,10-anthracene-9,10-endoperoxide dipropionate dianion that arises from a [2 + 4] cycloaddition of $^1O_2$ with 9,10-anthracene dipropionate dianion at pH = 10 in water detected by UV-visible spectroscopy.

Analytical methods such as low-temperature NMR spectroscopy can be used to detect unstable peroxide compounds in reaction mixtures. For example, dioxetane ^{13}C NMR signals are fairly characteristic (Baumstark, 1988b). Electron-rich olefins such as alkoxy-substituted alkenes react with singlet oxygen and form dioxetanes. Decomposition of dioxetanes is often accompanied by chemiluminescence due to a fragmented excited carbonyl compound (Adam and Trofimov, 2006; Turro *et al.*, 2010).

Singlet Oxygen Sensor Green (SOSG) is a $^1O_2$-specific fluorescent probe reagent that has been used to quantitatively measure $^1O_2$ that has been produced by determining the reaction rate of SOSG with $^1O_2$. SOSG is a fluorescein-anthracene die that fluoresces after its reaction with $^1O_2$. The endoperoxide product from a [2 + 4] cycloaddition of $^1O_2$ closes off the FRET quenching channel of precursor SOSG (Gollmer et al., 2011; Ragas et al., 2009). SOSG reacts with $^1O_2$ to produce SOSG endoperoxides, which emits a strong fluorescence signal at 531 nm. Φ_Δ has also been determined using SOSG for a porphyrin-based photosensitizer, hematoporphyrin monomethyl ether (Lin et al., 2013).

Fluorescence probes can also be used to detect highly reactive oxygen species such as hydroxyl radical (HO·) and reactive intermediates of peroxidase. 2-[6-(4′-hydroxy)phenoxy-3H-xanthen-3-on-9-yl]benzoic acid (HPF) and 2-[6-(4′-amino)phenoxy-3H-xanthen-3-on-9-yl]benzoic acid (APF) are two examples of such fluorescent probes (Setsukinai et al., 2003). Both probes are reported to be cell-permeable, relatively insensitive to superoxide anion, nitric oxide, $^1O_2$, and alkyl peroxides (Price et al., 2013; Price et al., 2009). APF is ~5 times more fluorescent during HO· formation than HPF (Price et al., 2009). Other fluorescent probes of hydroxyl radical include coumarin- and rhodamine nitroxide-based compounds (Meng et al., 2014; Yapici et al., 2012; Yuan et al., 2010).

Table 3 summarizes all methods available to determine rate constants and other photochemical parameters, along with whether or not the technique has been applied in an in-vivo model. The methods mentioned in this section can be useful tools to determine in-vivo and in-vitro photochemical parameters as well as characteristics of reactive species relevant for a specific photosensitizer. Based on this review, we consider the technique for fluorescence and SOLD-based lifetime (τ_f, τ_t, τ_Δ) measurements to be mature and able to accurately determine rate constants (k_1, k_2, k_3+k_5, k_4, k_6, k_7) as described in section 3.3. To determine k_3 and k_5, it is important to determine the triplet quantum yield, Φ_t, which can be determined using LIOAC. We also consider absorption measurements to be very mature and accurately determines the extinction coefficient e and k_0. However, the technique to determine the singlet oxygen quantum yield, Φ_Δ, is still dependent on the known reference singlet oxygen quantum yield, and thus may contain errors. Only indirect methods are available to determine Φ_Δ value in-vivo, which can be substantially different from the in-vitro value.

5. A review of existing values of photochemical parameters

Photosensitizers are normally delivered systemically or topically in PDT. The systemic administration involves either oral administration or intravenous injection so that the drug will be circulated through the whole body system, and preferentially more drug will be localized in the target site than in others. An ideal photosensitizer should have low or no toxicities and a fast clearance process. Some systemically delivered photosensitizers are benzoporphyrin derivative (BPD), Photofrin, and HPPH (2-[1-hexyloxyethyl]-2-devinyl pyropheophorbide-a). In contrast with the systemic administration, ALA, a pro-drug that reacts with heme to generate the photosensitizer protoporphyrin IX (PpIX), can also be applied topically to perform more localized delivery, which is commonly used for skin

treatment. Table 4 summarizes common photosensitizers that are currently used in various stages of clinical trials. Note that most of the PS are of type II category, with the exception of Tookad (WST-09) and WST-11, which are type I photosensitizers (Huang *et al.*, 2008).

There are several photosensitizers that have been approved for standard clinical use by the US Food and Drug Administration (FDA) or the European Medicines Agency (EMA) (Huang, 2005b; Agostinis *et al.*, 2011b). ALA (a prodrug that produces PpIX) was approved for the treatment of actinic keratoses in 1999by the FDA under the trade name Levulan (Jeffes, 2002) and in 2009 and 2011 by the EMA under the trade name Alacare and Ameluz, respectively. Similar photosensitizer derivatives were developed to also produce PpIX: methyl-ALA was approved by the FDA in 2004 for the treatment of non-hyperkeratotic actinic keratoses, and hexyl-ALA was approved in Europe in 2006for the diagnosis of bladder cancer under the trade name Hexvix (Lapini *et al.*, 2012). In 2000, the FDA approved use of BPD in treatment of age-related macular degeneration (Mody, 2000). *m*THPC was approved by the EMA for treatment of head and neck squamous cell carcinomas. Photofrin was approved by the FDA for multiple treatment sites. It was approved for microinvasive endobronchial non-small cell lung cancer in 1998and high-grade dysplasia in Barrett's esophagus in 2003.

The photochemical parameters, β, δ, ξ, σ, and g, can be determined using indirect methods mentioned previously (table 3) (Wang *et al.*, 2010; Liu *et al.*, 2013; Mitra and Foster, 2005). Currently only a subset of photosensitizers in table 5a (Photofrin, ALA, BPD, HPPH, mTHPC) have been studied. Every photosensitizer should undergo studies to determine the photochemical parameters so that they may be used for modeling the PDT process as well as dosimetry. The fundamental photophysical parameters of most, if not all, photosensitizers are fairly well established (e.g. ε, τ_f, τ_t), and they can be used to determine some parameters, such as ξ, for photosensitizers. However, indirect methods *in vivo* can only be used to determine the ratios of rate constants (k_i's, where $i = 1$–8), thus additional measurements are necessary to determine individual reaction rate constants. In this review, all parameters were determined for FDA or EMA approved photosensitizers (table 5a) as well as some others (table 5b). Table 5 summarizes the known values and references for the photosensitizers listed in table 4. Notice that this is a very incomplete list and includes only the most commonly and clinically used photosensitizers.

The photochemical parameters for most photosensitizers were determined *in vitro.* However, it is reasonable to expect that they will largely remain the same in *in vivo* systems (such as ε, k_0, k_3, and k_5). Thus, their values can be determined *in vitro* or *in vivo* for most photosensitizers. Some of the parameters (k_6, k_7) are photosensitizer independent since they are properties of either $^1O_2$ or other ROS and they should behave the same. Assumptions can be made that they are the same for all type II photosensitizers. Two of the photosensitizers summarized in this review are of type I, but it can be assumed that the corresponding parameters (k_6, k_1, k_8) are dependent only on the microenvironment and thus are approximately the same for different type I photosensitizers. Some photochemical parameters (k_1, k_2, k_4) are more environmentally dependent. Therefore it can be expected that the values for such parameters would be different between *in vivo* and *in vitro* conditions. One reason for this difference is due to aggregation which leads to

photosensitizer-photosensitizer photoreactions. It was found that the ratio β was roughly the same for all photosensitizers, which can help to estimate this value for unknown photosensitizers (Mitra and Foster, 2005).

This review of photochemical parameters indicates that some of the k_i's (k_2, k_4, k_6, k_7) are roughly of the same order of magnitude for all photosensitizers. Some of the k_i's (k_3, k_5) are the same order of magnitude for all type I or type II photosensitizers, but otherwise differ between the two types. Thus we believe they can be used to identify whether a particular photosensitizer will have type I or type II tendencies.

There are quite a number of photochemical parameters that is still unknown (see Table 5 for values either missing ('—') or estimated in parenthesis). Further studies are necessary to determine these values in-vivo directly. It is possible to expand the technology for direct method (Table 3) to be used in-vivo.

For BPD, the extinction coefficient (ε) was found to be 0.0783 cm^{-1} μM^{-1} using absorption spectroscopy (Aveline et al., 1994; Zhu et al., 2014). The value of k_0 was found at a fluence of 100 mW/cm^2 using Eq. (29) and ε. k_1 was found by using the approximation $k_1 \approx \sigma \cdot k_7[A]$, where σ is the specific photobleaching ratio determined in-vivo using SOED in Section 4.2.2. Using the definition of $\sigma = k_1 \tau_\Delta$, k_1 was calculated by $\sigma \cdot \tau_\Delta = \sigma(k_1([S_0]+\delta)+k_6) \approx \sigma \cdot k_7[A]$ with the approximation that $k_7[A] \gg (k_1([S_0]+\delta)+k_6)$. k_2 was found to be 3×10^3 μM^{-1}s^{-1} using the observed triplet lifetime (τ_t) in the presence and absence of $^3O_2$ (Eq. (34)) (Aveline et al., 1994). Using this value, and the measured value for β in-vivo, k_4 can be found to be $k_4 = \beta \times k_2 = (11.9 \text{ μM}) \times (3\times10^3 \text{ μM}^{-1}\text{s}^{-1}) = 3.6\times10^4$ s^{-1}. The values for k_3 and k_5 were found by using the fluorescence lifetime (τ_f) and the triplet quantum yield (Φ_t) and Eqs. (31)-(33). The value of τ_f was taken from literature Aveline et al. using a time-correlated single photon counting method (Aveline et al., 1994). The value of Φ_t was obtained from literature using LIOAC (see Table 3 and section 4) (Aveline et al., 1994). The resulting values were $k_3 = (1-\Phi_t)/\tau_f = (1-0.79)/(5.2\times10^{-9} \text{ s}) = 4.04\times10^7$ s^{-1} and $k_5 = \Phi_t/\tau_f = 0.79/5.2\times10^{-9}$ s $=1.52\times10^7$ s^{-1}. The singlet oxygen lifetime (τ_Δ) in water with no acceptors to react with $^1O_2$ can be used with Eq. (30) to obtain the value of k_6, which is only a property of singlet oxygen and should be photosensitizer independent. Therefore, for all type II photosensitizers, $k_6 = \tau_\Delta^{-1} = (3 \text{ μs})^{-1} = 3.3\times10^5$ s^{-1} (Zhu et al., 2015a). The value of $k_7[A]$ in-vivo is only a property of singlet oxygen and is thus assumed to be the same for all type II photosensitizers. By using the value of τ_Δ in tissue (0.1 μs) and the known value for k_6, $k_7 = \tau_\Delta^{-1} - k_6 = (0.1 \text{ μs})^{-1} - (3.3\times10^5 \text{ s}^{-1}) = 1\times10^7$ s^{-1} (Dysart et al., 2005). Since BPD is a type II photosensitizer, there is no significant contribution of type I reactions between [T1] and [A] so $k_8[A]$ and η were assumed to be 0. The values of ξ, σ, and g were found in-vivo using SOED method (Kim et al., 2015a; Kim et al., 2014a; McMillan et al., 2013; Zhu et al., 2015a). Details for the SOED method are in section 4.2.2. The low concentration correction, δ, was assumed to be the same for BPD as that of Photofrin. Further experiments are needed to confirm this value for BPD. The fraction of $^1O_2$ producing reactions between [T] and $^3O_2$ was determined using the definition of ξ in table 2: $S_\Delta = \xi/\Phi_t/\varepsilon x(h\nu) = (51\times10^{-3}$ cm^{2}mW^{-1}s^{-1})/(0.79)/(0.0312 μM^{-1}cm^{-1}) $\times$ (6.022$\times10^{14}$ cm^{3}μM^{-1}) $\times$ (2.72 $\times10^{-16}$ mW s) = 0.144.

6. Conclusions

During PDT, energy from the triplet-state photosensitizer excited via the absorption of light is transferred to ground-state oxygen, which produces ROS. Mathematical models have been developed to simulate the process of PDT for both type I and II photosensitizers. These models use a set of differential equations describing the major photochemical reaction pathways in PDT to calculate temporal and spatial distributions of singlet oxygen, ground-state oxygen, and the photosensitizer.

This review summarizes the known values for the photochemical parameters and methods to determine the rate constants and other key photochemical parameters *in-vivo*. It is found that many fundamental rate constant values are unavailable for many common photosensitizers, and experimental efforts to determine these parameters are required in order to perform explicit dosimetry of ROS.

There is great potential for future work to determine *in-vivo* photochemical rate parameters for use in PDT modeling and dosimetry. However, further studies are needed to determine these parameters *in vivo*. For a particular photosensitizer to be studied in pre-clinical and clinical dosimetry studies, it is important to have the complete set of photophysical and photochemical parameters.

Acknowledgments

Appendix A: Biological and Other Examples of Singlet Oxygen Reactions

Important biological building-blocks such as imidazole or DNA base pairs like guanine, react with $^1O_2$ by [2 + 4] cycloaddition to form endoperoxide which can be characterized at low temperature (Sheu and Foote, 1993).

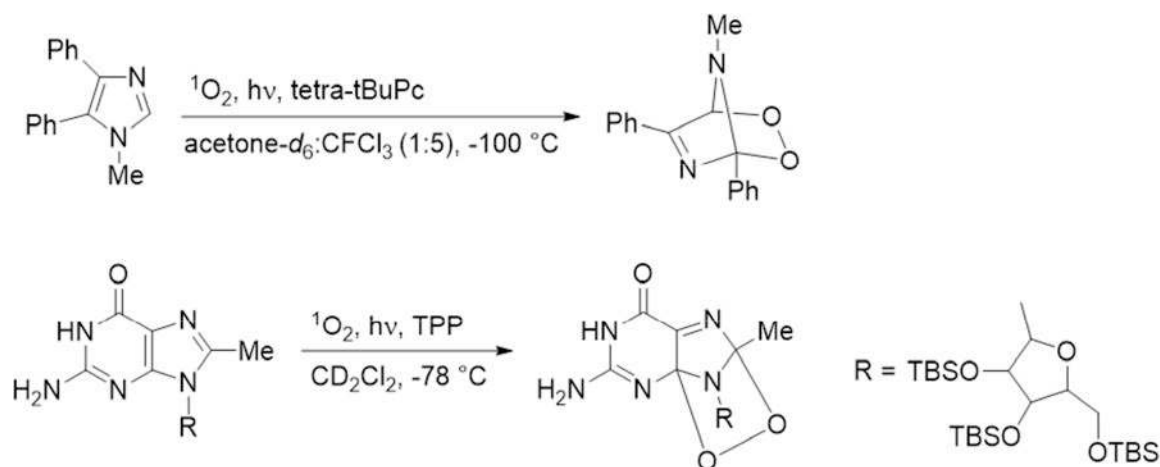**Figure A1.**

Reaction of imidazole (top) and guanine (bottom) with $^1O_2$ to form endoperoxides. tetra-tBuPc = tetra-tert-butylphthalocyanines and TPP = tetraphenylporphyrin photosensitizers, CD_2Cl_2 = chloroform-d_2 and $CFCl_3$ = trichlorofluoromethane solvent.

DNA base pairs can also undergo tandem photooxidation with $^1O_2$ to form spirodiimidohydantoin species (McCallum *et al.*, 2004; Di Mascio *et al.*, 2014; Hickerson *et al.*, 1999).
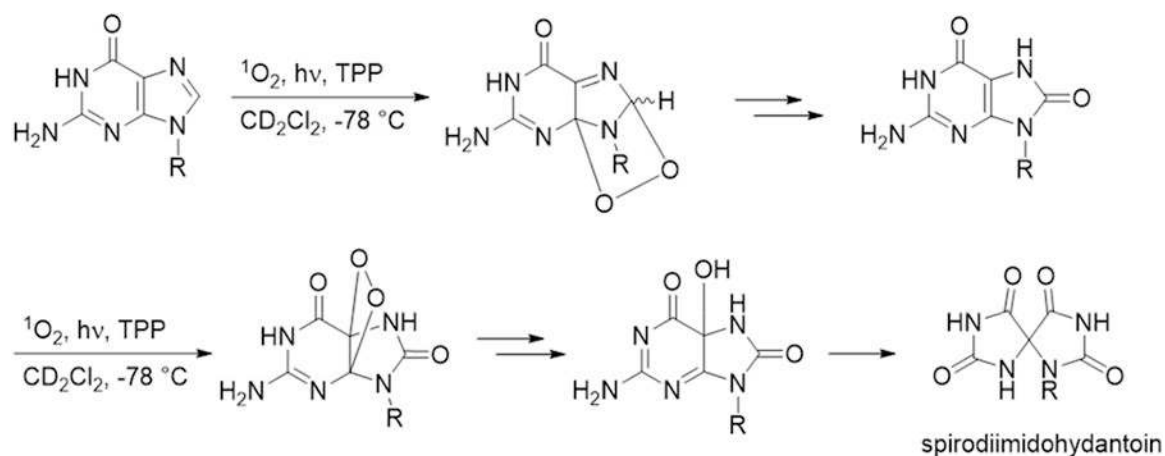

Figure A2.
Reaction of DNA basepairs with $^1O_2$ to form spirodiimidohydantoin. TPP = tetraphenylporphyrin photosensitizer and CD_2Cl_2 = chloroform-d_2 solvent.

Conjugated dienes undergo tandem photooxidation with $^1O_2$ to form allylic hydroperoxides followed by 1,4-endoperoxides. These kinds of conjugated alkenes are common in natural products and lipids in biological systems (Blay *et al.*, 2005).

4α-hydroxy peroxyguaienes
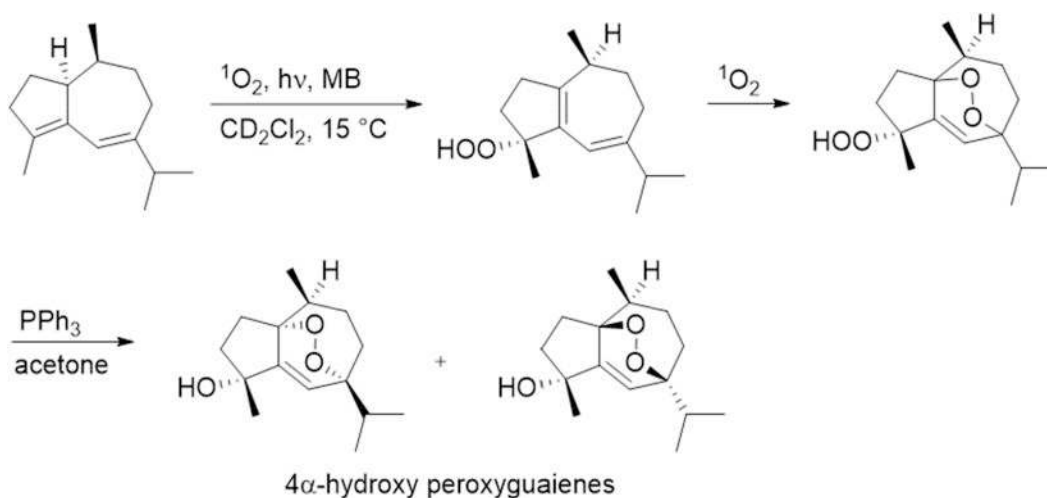
Figure A3.

Reaction of conjugated dienes with $^1O_2$ to form allylic hydroperoxides, followed by 1,4-endoperoxides. MB = methylene blue photosensitizer, CD_2Cl_2 = chloroform-d_2 solvent and PPh_3 = triphenylphosphine.

Singlet oxygen reacts with electron-rich alkene by [2 + 2] cycloadditions to give mono and bis bicyclic dioxetanes which chemiluminesce on decomposition (Zaklika *et al.*, 1978; Adam *et al.*, 1979).
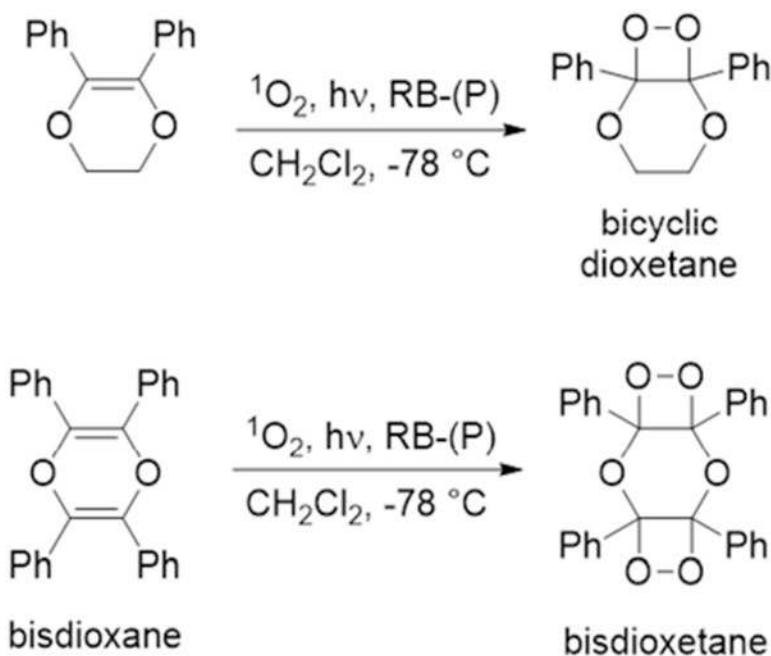

Figure A4.
Top: reaction of alkene with $^1O_2$ to form bicyclic dioxetanes. Bottom: Reaction of bisdioxane with $^1O_2$ to form bisdioxefane. RB-(P) = Rose Bengal photosensitizer immobilized on polymer support and CH_2Cl_2 = dichloromethane solvent.

Highly conjugated aromatic groups react with $^1O_2$ by [2 + 4] cycloaddition mechanism to give endoperoxide which also acts as a chemical source of $^1O_2$ eg. naphthalene, anthracene (Wasserman and Larsen, 1972; Fudickar and Linker, 2014; Klaper and Linker, 2015).

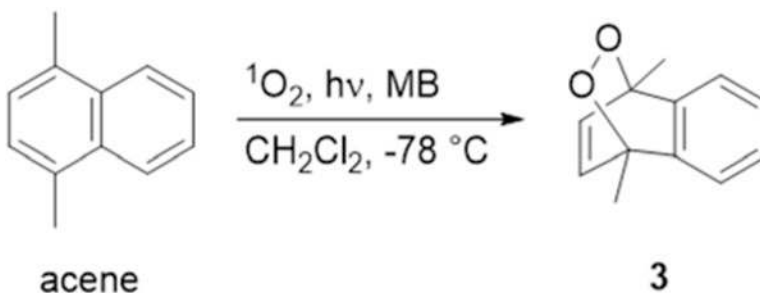**Figure A5.**

Reaction of acene with $^1O_2$ to form endoperoxide. MB = methylene blue photosensitizer and CH_2Cl_2 = dichloromethane solvent.

Photosensitizers such as dyes, pharmaceuticals, and cosmetics can serve as photodynamic agents and produce $^1O_2$. A variety of chromophore-rich natural products can sensitize organisms to damage by singlet oxygenation, including chlorophyll, metal-less porphyrins, flavins, polyacetylenes, pigments, and mold toxins.(Wasserman, 1979).

Appendix B: Microscopic Singlet Oxygen Model

With the microscopic singlet oxygen model, the tumor is assumed to have uniformly distributed capillaries aligned parallel to the linear light source. The inter-capillary distance between two adjacent capillaries is large enough so that each one can supply oxygen only to its immediate, concentric surrounding tissue. A Krogh cylinder model can be adapted for a single capillary and its surrounding tissue. The three-dimensional Krogh model can be simplified into a two-dimensional, cylindrically symmetric model. Under normal situations, the red blood cell (RBC) contains hemoglobin, which is where hemoglobin saturation and desaturation occurs. After oxygen unloads from oxy-hemoglobin, it will diffuse into the blood through the RBC membrane and into the tissue. The microscopic model assumes that there is no oxygen diffusion barrier in the RBC membrane, and that the distribution of hemoglobin within the capillary is uniform. Given these assumptions, the time-dependent governing equations for $^3O_2$ and hemoglobin transport inside the capillary are given by (Zhu *et al.*, 2015c):

$$\alpha_c \frac{\partial P}{\partial t} = \alpha_c D_c \nabla^2 P - v \cdot \alpha_c \nabla P + \Gamma_{ox}; \quad \text{(B1)}$$

$$C_H \frac{\partial Sa}{\partial t} = C_H D_H \nabla^2 Sa - v \cdot C_H \nabla Sa - \Gamma_{ox}; \quad \text{(B2)}$$

where *Sa* denotes the hemoglobin oxygen saturation describing the percentage of hemoglobin oxygen concentration to the total hemoglobin concentration. Γ_{ox} is the "reaction" term representing the $^3O_2$ loading/unloading from deoxyhemoglobin/oxyhemoglobin. D_c and D_h represent the diffusion coefficients of $^3O_2$ and hemoglobin in the capillary respectively. a_c is the solubility of $^3O_2$ in plasma and *v* is the blood velocity in the capillary. The concentration of $^3O_2$ is expressed using the partial pressure (*P*) of $^3O_2$ and the oxygen solubility coefficient (*a*) based on

$$\lceil ^3O_2 \rceil = \alpha P. \quad \text{(B3)}$$

Oxygen concentration can be expressed using oxygen partial pressure. The oxygen supply term (Γ) for equation (18) is given by

$$\Gamma = D_t \nabla^2 [^3O_2] - q_0 \frac{[^3O_2]}{[^3O_2] + \alpha_t P_m}. \quad \text{(B4)}$$

where q_0 is the maximum metabolic oxygen consumption rate in the Michaelis-Menten relationship (Hudson and Cater, 1964) for the microscopic model, D_t is the $^3O_2$ diffusion coefficient in tissue, and P_m is the $^3O_2$ partial pressure at half maximum $^3O_2$ consumption concentration. As well as in a vascular medium:

$$\Gamma = D_s \nabla^2 [^3O_2], \quad \text{(B5)}$$

where D_s is the $^3O_2$ diffusion coefficient in vascular media.

Unless the microscopic vascular structures are known or important for the purpose of the model, it is often unnecessary to model the oxygen diffusion process if the vessels are assumed to be uniformly distributed because the oxygen diffusion typically happens at a spatial scale of less than 50 μm and the details of oxygen diffusion have little impact on light transport or drug distribution, which often happen in the mm spatial scale. Microscopic modeling should explain subtle details of tissue reoxygenation after interruptions of the light irradiation at appropriate intervals (fractionated PDT), which may not be completely modeled in a macroscopic model.

References

Adam W. The Singlet Oxygen Story. Chemie in unserer Zeit. 1981; 15:190–6.

Adam W, Cheng CC, Cueto O, Erden I, Zinner K. A stable bisdioxetane. J Am Chem Soc. 1979; 101:4735–6.

Adam, W., Trofimov, A. Chemistry of Peroxides. Rappoport, Z., editor. Vol. 2. 2006. p. 1171-209.

Agostinis P, Berg K, Cengel KA, Foster TH, Girotti AW, Gollnick SO, Hahn SM, Hamblin MR, Juzeniene A, Kessel D, Korbelik M, Moan J, Mroz P, Nowis D, Piette J, Wilson BC, Golab J. Photodynamic therapy of cancer: An update. CA: Cancer J Clin. 2011a; 61:250–81. [PubMed: 21617154]

Agostinis P, Berg K, Cengel KA, Foster TH, Girotti AW, Gollnick SO, Hahn SM, Hamblin MR, Juzeniene A, Kessel D, Korbelik M, Moan J, Mroz P, Nowis D, Piette J, Wilson BC, Golab J. Photodynamic Therapy of Cancer: An Update. CA Cancer J Clin. 2011b; 61:250–81. [PubMed: 21617154]

Arnfield MR, Chapman JD, Tulip J, Fenning MC, PMcPhee MS. Optical properties of experimental prostate tumors in vivo. Photochem Photobiol. 1993; 57:306–11. [PubMed: 8451295]

Arnold SJ, Ogryzlo EA, Witzke H. Some New Emission Bands of Molecular Oxygen. J Chem Phys. 1964; 40:1769–70.

Aubry JM, Pierlot C, Rigaudy J, Schmidt R. Reversible bindig of oxygen to aromatic compounds. Acc Chem Res. 2003; 36:668–75. [PubMed: 12974650]

Aveline BM, Hasan T, Redmond RW. Photophysical and photosensitizing properties of benzoporphyrin derivative monoacid ring A (BPD-MA). Photochem Photobiol. 1994; 59:328–35. [PubMed: 8016212]

Aveline BM, Sattler RM, Redmond RW. Environmental Effects on Cellular Photosensitization: Correlation of Phototoxicity Mechanism with Transient Absorption Spectroscopy Measurements. Photochem Photobiol. 1998; 68:51–62. [PubMed: 9679451]

Azab M, DBoyer DS, Bressler NM, et al. Verteporfin therapy of subfoveal minimally classic choroidal neovascularization in age-related macular degeneration: 2-year results of a randomized clinical trial. Arch Opthalmol. 2005; 123:448–57.

Baron ED, Malbasa CL, Santo-Domingo D, Fu P, Miller JD, Hannerman KK, Hsia AH, Oleinick L, Colussi VC, Cooper KD. Silicon phthalocyanine (pc 4) photodynamic therapy is a safe modality for cutaneous neoplasms: results of a phase 1 clinical trial. Laser Surg Med. 2010; 42:888–95.

Baumstark, AL. Advances in Oxygenated Processes. Baumstark, AL., editor. Greenwich, CT: JAI Press; 1988a. p. 31-84.

Baumstark, AL. Advances in Oxygenated Processes. Baumstark, AL., editor. Greenwich, CT: JAI Press; 1988b. p. 31-84.

Bellnier DA, Greco WR, Loewen GM, Nava H, Oseroff AR, Pandey RK, Tsuchida T, Dougherty TJ. Population pharmacokinetics of the photodynamic therapy agent 2-[1-hexyloxyethyl]-2-devinyl pyropheophorbide-a in cancer patients. Cancer Res. 2003; 63:1806–13. [PubMed: 12702566]

Bensasson R, Chachaty C, Land EJ, Salet C. Nanosecond irradiation studies of biological molecules - I. coenzyme Q 6 (ubiquinone-30). Photochem Photobiol. 1972; 16:27–37. [PubMed: 5037228]

Blay G, Garcia B, Molina E, Pedro JR. Total syntheses of four stereoisomers of 4a-hydroxy-1b,7b-peroxy-10bH-guaia-5-ene. Org Lett. 2005; 7:3291–4. [PubMed: 16018643]

Bonnet R, Lambert C, Land EJ, Scourides PA, Sinclair RS, Truscott TG. The triplet and radical species of hematoporphyrin and some of its radical species. Photochem Photobiol. 1983; 38:1–8. [PubMed: 6622548]

Braslavsky SE, Heibel GE. Time-resolved photothermal and photoacoustic methods applied to photoinduced processes in solution. Chem Rev. 1992; 92:1381–410.

Cadet J, Ravanat J-L, Martinez GR, Medeiros MGH, Di Mascio. Singlet Oxygen Oxidation of Isolated and Cellular DNA: Product Formation and Mechanistic Insights. Photochem Photobiol. 2006; 82:1219–25. [PubMed: 16808595]

Catalan J, Diaz C, Barrio L. Analysis of mixed solvent effects on the properties of singlet oxygen (1 Δ g). Chem Phys. 2003; 300:33–9.

Celaje JA, Zhang D, Guerrero AM, Selke M. Chemistry of trans-Resveratrol with Singlet Oxygen: [2 + 2] Addition, [4 + 2] Addition, and Formation of the Phytoalexin Moracin M. Org Lett. 2011; 13:4846–9. [PubMed: 21859123]

Chakraborty A, Held KD, Prise KM, Liber HL, Redmond RW. Bystander Effects Induced by Diffusing Mediators after Photodynamic Stress. Radiat Res. 2009; 172:74–81. [PubMed: 19580509]

Chattopadhyay SK, Kumar CV, Das PK. Laser flash photolytic determination of triplet yields via singlet oxygen generation. J Photochem. 1984; 24:1–9.

Chen B, Pogue BW, Zhou X, O'Hara JA, Solban N, Demidenko E, Hoopes PJ, Hasan T. Effect of Tumor Host Microenvironment on Photodynamic Therapy in a Rate Prostate Tumor Model. Clin Cancer Res. 2005; 11:720–7. [PubMed: 15701861]

Chen Q, Wilson BC, Shetty SD, Patterson MS, Cerny JC, Hetzel FW. Changes in in vivo optical properties and light distributions in normal canine prostate during photodynamic therapy. Radiat Res. 1997; 147:86–91. [PubMed: 8989374]

Clennan EL, Dobrowolski P, Greer A. Reaction of Singlet Oxygen with Thietane. A Novel Example of a Self-Catalyzed Reaction Which Provides Evidence for a Thiadioxirane Intermediate. J Am Chem Soc. 1995; 117:9800–3.

Clennan, EL., Foote, CS. Organic Peroxides. Ando, W., editor. Chichester, UK: Wiley; 1992. p. 255-318.

Cox GS, Bobillier C, Whitten DG. Photooxidation and singlet oxygen sensitization by protoporphyrin IX and its photooxidation products. Photochem Photobiol. 1982; 36:401–7.

Cox GS, Whitten DG. Mechanisms for the Photooxidation of Protoporphyrin IX in Solution. J Am Chem Soc. 1982; 104:516–21.

Cuenca RE, Allison RR, Sibata C, Downie GH. Breast cancer with chest wall progression: treatment with photodynamic therapy. Ann Surg Oncol. 2004; 11:322–7. [PubMed: 14993029]

Demas JN, Crosby GA. The Measurement of Photoluminescence Quantum Yields. Review. J Phys Chem. 1971; 75:991–1024.

Di Mascio, P., Miyamoto, S., Medeiros, MGH., Martinez, GR., Cadet, J. Chemistry Functional Groups in Organic Chemistry - The Chemistry of Peroxides 3. Patai, S., Rappoport, Z., editors. 2014. p. 769-804.

Dougherty TJ. Photodynamic Therapy. Photochem Photobiol. 1993; 58:896–900.

Dragieva G, Hafner J, Dummer R, Schmid-Grendelmeier P, Roos M, Prinz BM, Burg G, Binswanger U, Kempf W. Topical photodynamic therapy in the treatment of actinic keratoses and Bowen's diseas in transplant recipients. Transplantation. 2004; 151:196–200.

Dysart JS, Patterson MS. Characterization of Photofrin photobleaching for singlet oxygen dose estimation during photodynamic therapy of MLL cells in vitro. Phys Med Biol. 2005; 50:2597–616. [PubMed: 15901957]

Dysart JS, Patterson MS. Photobleaching kinetics, photoproduct formation, and dose estimation during ALA induced PpIX PDT of MLL cells under well oxygenated and hypoxic conditions. Photochem Photobiol Sci. 2006; 5:73–81. [PubMed: 16395430]

Dysart JS, Singh G, Patterson MS. Calculation of singlet oxygen dose from photosensitizer fluorescence and photobleaching during mTHPC photodynamic therapy of MLL cells. Photochem Photobiol. 2005; 81:196–205. [PubMed: 15469385]

Ericson MB, Sandberg C, Stenquist B, Gudmunson F, Karisson M, Ros A-M, Rosen A, Larko O, Wennberg A-M, Rosdahl I. Photodynamic therapy of actinic keratosis at varying fluence rates: assessment of photobleaching, pain and primary clinical outcome. Br J Dermatol. 2004; 151:1204–12. [PubMed: 15606516]

Fernandez JM, Bilgin MD, Grossweiner LI. Singlet oxygen generation by photodynamic agents. J Photochem Photobiol B. 1997; 37:131–40.

Finlay JC, Conover DL, Hull EL, Foster TH. Porphyrin Bleaching and PDT-induced Spectral Changes are Irradiance Dependent in ALA-sensitized Normal Rat Skin In Vivo. Photochem Photobiol. 2001; 73:54–63. [PubMed: 11202366]

Finlay JC, Mitra S, Patterson MS, Foster TH. Photobleaching kinetics of Photofrin in vivo and in multicell tumour spheroids indicate two simultaneous bleaching mechanisms. Phys Med Biol. 2004; 49:4837–60. [PubMed: 15584523]

Finlay JC, Zhu TC, Dimofte A, Stripp D, Malkowicz SB, Busch TM, Hahn SM. Interstitial Fluorescence Spectroscopy in the Human Prostate During Motexafin Lutetium-Mediated Photodynamic Therapy. Photochem Photobiol. 2006; 82:1270–8. [PubMed: 16808592]

Foote, CS. Free Radicals in Biology. Pryor, WA., editor. New York: Academic Press; 1976. p. 85-133.

Foote CS. Definition of type I and type II photosensitized oxidation. Photochem Photobiol. 1991; 54:659. [PubMed: 1798741]

Foster TH, Hartley DF, Nichols MG, Hilf R. Fluence Rate Effects in Photodynamic Therapy of Multicell Tumor Spheroids. Cancer Res. 1993; 53:1249–54. [PubMed: 8443805]

Foster TH, Murant RS, Bryant RG, Knox RS, Gibson SL, Hilf R. Oxygen Consumption and Diffusion Effects in Photodynamic Therapy. Radiat Res. 1991; 126:296–303. [PubMed: 2034787]

Fudickar, W., Linker, T. Patai's Chemistry of Functional Groups. Patai, S., Rappoport, Z., editors. 2014. p. 21-86.

Fuwa K, Valle BL. The Physical Basis of Analytica Atomic Absorption Spectrometry. The Pertinence of the Beer-Lambert Law. Anal Chem. 1963; 35:942–6.

Georgakoudi I, Foster TH. Singlet Oxygen- Versus Nonsinglet Oxygen-Mediated Mechanisms of Sensitizer Photobleaching and Their Efects on Photodynamic Dosimetry. Photochem Photobiol. 1998; 67:612–25. [PubMed: 9648527]

Georgakoudi I, Nichols MG, Foster TH. The Mechanism of Photofrin Photobleaching and Its Consequences for Photodynamic Dosimetry. Photochem Photobiol. 1997; 65:135–44. [PubMed: 9066293]

Girotti, AW. Comprehensive Series in Photosciences. PU, Giacomoni, editor. Elsevier; 2001. p. 233-50.

Gollmer A, Arnbjerg J, Blaikie FH, Wett Pedersen B, Breitenbach T, Daasbjerg K, Glasius M, Ogilby PR. Singlet Oxygen Sensor Green: Photchemical Behavior in Solution and in a Mammalian Cell. Photochem Photobiol. 2011; 87:671–9. [PubMed: 21272007]

Gollnick K. Type II photooxygenation reactions in solution. Adv Photochem. 1968; 6

Greer A. Christopher Foote's Discovery of the Role of Singlet Oxygen [1O2 (1 Δ g)] in Photosensitized Oxidation Reactions. Acc Chem Res. 2006; 39:797–804. [PubMed: 17115719]

Greer, A., Balaban, AT., Liebman, JF. The Chemistry of Peroxides. Vol. 3. Wiley; 2014.

Guldi DM, Mody TD, Gerasimchuk NN, Magda D, Sessler JL. Influence of Large Metal Cations on the Photophysical Properties of Texaphyrin, a Rigid Aromatic Chromophore. J Am Chem Soc. 2000; 122:8289–98.

Hadjur C, Lange N, Rebstein J, Monnier P, van den Bergh H, Wagnieres G. Spectroscopic studies of photobleaching and photoproduct formation of meta(tetrahydroxyphenyl)chlorine (m-THPC) used in photodynamic therapy. The production of singlet oxygen by m-THPC. J Photochem Photobiol B. 1998; 45:170–8.

Hage M, Siersema PD, van Dekken H, Steyerberg EW, Haringsma J, van de Vrie W, Grool TE, van Veen RLP, Sterenborg HJCM, Kulpers EJ. Aminolevulinic acid photodynamic therapy versus argon plasma coagulation for ablation of Barrett's oesophagus: a randomised trial. Gut. 2004; 53:785–90. [PubMed: 15138203]

He J, Larkin HE, Li Y-S, Rihter BD, Zaidi SIA, Rodgers MAJ, Mukhtar H, Kenney ME, Oleinick L. The Synthesis, Photophysical and Photobiological Properties and in vitro Structure-Activity Relationships of a Set of Silicon Phthalocyanine PDT Photosensitizers. Photochem Photobiol. 1997; 65:581–6. [PubMed: 9077144]

Hickerson RP, Prat F, Muller JG, Foote CS, Burrows CJ. Sequence and Stacking Dependence of 8-Oxoguanine Oxidation: Comparison of One-Electron vs Singlet Oxygen Mechanisms. J Am Chem Soc. 1999; 121:9423–8.

Higgins, R., Foote, CS., Cheng, H. Advances in Chemistry. Gould, RF., editor. Washington DC: American Chemical Society; 1968. p. 102-17.

Hirano T, Kohno E, Nishiwaki M. Detection of near infrared emission from singlet oxygen in PDT with an experimental tumor bearing mouse. J Jpn Soc Laser Surg Med. 2002; 22:99–108.

XH, Hu, Feng, Y., Lu, JQ., Allison, RR., Cuenca, RE., Downie, GH., Sibata, CH. Modeling of a Type II Photofrin-mediated Photodynamic Therapy Process in a Heterogeneous Tissue Phantom. Photochem Photobiol. 2005a; 81:1460–8. [PubMed: 15960591]

Hu XH, Feng Y, Lu JQ, Allison RR, Cuenca RE, Downie GH, Sibata CH. Modeling of a Type II Photofrin-mediated Photodynamic Therapy Process in a heterogeneous tissue phantom. Photochem Photobiol. 2005b; 81:1460–8. [PubMed: 15960591]

Huang Z. A Review of Progress in Clinical Photodynamic Therapy. Technol Cancer Res Treat. 2005a; 4:283–93. [PubMed: 15896084]

Huang Z. A Review o Progress in Clinical Photodynamic Therapy. Technol Cancer Res Treat. 2005b; 61:283–93.

Huang Z, Xu H, Meyers AD, Musani AI, Wang L, Tagg R, Barqawi AB, Chen YK. Photodynamic Therapy for Treatment of Solid Tumors - Potential and Technical Challenges. Technol Cancer Res Treat. 2008; 7:309–20. [PubMed: 18642969]

Hudson JA, Cater DB. An analysis of factors affecting tissue oxygen tension. Proc R Soc London B. 1964; 161:247–74. [PubMed: 14224411]

Hurst JR, McDonald JD, Schuster GB. Lifetime of singlet oxygen in solution directly determined by laser spectroscopy. J Am Chem Soc. 1982; 104:2065–7.

Igbaseimokumo U. Quantification of in vivo Photofrin uptake by human pituitary adenoma tissue. J Neurosurg. 2004; 101:272–7. [PubMed: 15309918]

Itri R, Junqueira HC, Mertins O, Babtista MS. Membrane Changes Under Oxidative Stress: The Impact of Oxidized Lipids. Biophys Rev. 2014; 6:47–61. [PubMed: 28509959]

Jarvi MT, Niedre MJ, Patterson MS, Wilson BC. Singlet Oxygen Luminescence Dosimetry (SOLD) for Photodynamic Therapy: Current Status, Challenges and Future Prospects. Photochem Photobiol. 2006; 82:1198–210. [PubMed: 16808593]

Jarvi MT, Niedre MJ, Patterson MS, Wilson BC. The Influences of Oxygen Depletion and Photosensitizer Triplet-state Dynamic During Photodynamic Therapy on Accurate Singlet Oxygen Luminescence Monitoring and Analysis of Treatment Dose Response. Photochem Photobiol. 2011; 87:223–34. [PubMed: 21143603]

Jeffes EWB. Levulan®: the first approved topical photosensitizer for the treatment of actinic keratosis. J Dermatol Treat. 2002; 13:s19–s23.

Jensen RL, Arnbjerg J, Ogilby PR. Temperature effects on the solvent-dependent deactivation of singlet oxygen. J Am Chem Soc. 2010; 132

Johansson A, Svensson J, Andersson-Engels S, Bendsoe N, Svanberg K, Bigio I, Alexandratou E, Kyriazi M, Yova D, Grafe S, Trebst T. mTHPC pharmacokinetics following topical administration. Proc SPIE. 2006; 6094:6094C1-C-8.

Josefsen LB, Boyle RW. Photodynamic Therapy and the Development of Metal-Based Photosensitis. Met Based Drugs. 2008; 2008:1–24.

Kanofsky JR. Singlet Oxygen Production by Biological Systems. Chem Biol Interac. 1989; 70:1–28.

Kanofsky JR. Quenching of singlet oxygen by human plasma. Photochem Photobiol. 1990; 51:299–303. [PubMed: 2356225]

Kasha, M. Singlet O2. Frimer, AA., editor. Boca Raton, FL: CRC Press; 1985. p. 1-12.

Kato H, Furukawa K, Sato M, Okunaka T, Kusunoki Y, Kawahara M, Fukuoka M, Miyazawa T, Yana T, Matsui K, Shiraishi T, Horinouchi H. Phase II clinical study of photodynamic therapy using mono-l-aspartyl chlorin e6 and diode laser for early superficial squamous cell carcinoma of the lung. Lung Cancer. 2003; 42:103–11. [PubMed: 14512194]

Kelty CJ, Ackroyd R, Brown NJ, Brown SB, Reed MW. Comparison of high- vs low-dose 5-aminolevulinic acid for photodynamic therapy of Barrett's esophagus. Surg Endosc. 2004; 18:452–8. [PubMed: 14752635]

Kennedy JC, Pottier RH. Endogenous protoporphyrin IX, a clinically useful photosensitizer for photodynamic therapy. J Photochem Photobiol B: Biol. 1992; 14:275–92.

Khan AU, Kasha M. Red Chemiluminescence of Molecular Oxygen in Aqueous Solution. J Chem Phys. 1963; 39:2105–6.

Khan AU, Kasha M. Rotational Structure in the Chemiluminescence Spectrum of Molecular Oxygen in Aqueous Systems. Nature. 1964; 204:241–3.

Khan AU, Kasha M. Chemiluminescence arising from simultaneous transitions in pairs of singlet oxygen molecules. J Am Chem Soc. 1970; 92:3293–300.

Khan AU, Kasha M. Direct spectroscopic observation of singlet oxygen emission at 1268 nm excited by sensitizing dyes of biological interest in liquid solution. Proc Nat Acad Sci. 1979; 76:6047–9. [PubMed: 16592729]

Kim MM, Finlay JC, Zhu TC. Macroscopic singlet oxygen model incorporating photobleaching as an input parameter. Proc SPIE. 2015a; 9308:93080V-1-6.

Kim MM, Liu B, Miller J, Busch TM, Zhu TC. Parameter determination for BPD-mediated vascular PDT. Proc SPIE. 2014a; 8931:89311D-1-6.

Kim MM, Penjweini R, Zhu TC. In vivo outcome study of BPD-mediated PDT using a macroscopic singlet oxygen model. Proc SPIE. 2015b; 9308:93080A-1-8.

Kim S, Ohulchanskyy TY, Pudavar HE, Pandey RK, Prasad PN. Organically Modified Silica Nanoparticles Co-encapsulating Photosensitizing Drug and Aggregation-Enhanced Two-Photon Absorbing Fluorescent Dye Aggregates for Two-Photon Photodynamic Therapy. J Am Chem Soc. 2007; 129:2669–75. [PubMed: 17288423]

Kim S, Tachikawa T, Fujitsuka M, Majima T. Far-Red Fluorescence Probe for Monitoring Singlet Oxygen during Photodynamic Therapy. J Am Chem Soc. 2014b; 136:11707–15. [PubMed: 25075870]

Kinsella TJ, Baron ED, Colussi VC, Cooper KD, Hoppel CL, Ingalls ST, Kenney ME, Li X, Oleinick L, Stevens SR, Remick SC. Preliminary clinical and pharmacologic investigation of photodynamic

therapy with the silicon phthalocyanine photosensitizer Pc 4 for primary or metastatic cutaneous cancers. Front Oncol. 2011; 1:1–6. [PubMed: 22655224]

Klaper M, Linker T. Intramolecular Transfer of Singlet Oxygen. J Am Chem Soc. 2015; 137:13744–7. [PubMed: 26474239]

Konig K, Schneckenburger H, Ruck A, Steiner R. In vivo photoproduct formation during PDT with ALA_induced endogenous porphyrins. J Photochem Photobiol B. 1993; 18:287–90. [PubMed: 8350194]

Kotani H, Ohkubo K, Fukuzumi S. Photocatalytic oxygenation of anthracenes and olefins with dioxygen via selective radical coupling using 9-mesityl-10-methylacridinium ion as an effective electron-transfer photocatalyst. J Am Chem Soc. 2004; 126:15999–6006. [PubMed: 15584734]

Krammer B, Plaetzer K. ALA and its clinical impact, from bench to bedside. Photochem Photobiol Sci. 2008; 7:283–9. [PubMed: 18389144]

Krasnovskii AA. Photosensitized Luminescence of Singlet Oxygen in Solution. Biofizika. 1976; 21:748–9. [PubMed: 1009166]

Kress M, Meier T, Steiner R, Dolp F, Erdmann R, Ortmann U, Ruck A. Time-resolved microspectrofluorometry and fluorescence lifetime imaging of photosensitizers using picosecond pulsed diode lasers in laser scanning microscopes. J Biomed Opt. 2003; 8:26–32. [PubMed: 12542376]

Krieg M, Redmond RW. Photophysical properties of 33'-dialkylthiacarbocyanine dyes in homogeneous solution. Photochem Photobiol. 1993; 57:472–9. [PubMed: 8475181]

Krieg M, Srichai MB, Redmond RW. Photophysical properties of 33'-dialkylthiacarbocyanine dyes in organized media: unilamellar liposomes and thin polymer films. Biochim Biophys Acta. 1993a; 1151:168–74. [PubMed: 8373793]

Krieg M, Srichai MB, Redmond RW. Photophysical properties of 33′-dialkylthiacarbocyanine dyes in organized media: unilamellar liposomes and thin polymer films. Biochim Biophys Acta. 1993b; 1151:168–74. [PubMed: 8373793]

Lakowicz JR, Szmacinski H, Nowaczyk K, Berndt KW, Johnson M. Fluorescence lifetime imaging. Anal Biochem. 1992; 202:316–30. [PubMed: 1519759]

Lapini A, Minervini A, Masala A, Schips L, Pycha A, Cindolo L, Giannella R, Martini T, Vittori G, Zani D, Bellomo F, Cosciani Cunico S. A comparison of hexaminolevulinate (Hexvix) fluorescence cystoscopy and white-light cystoscopy for detection of bladder cancer: results of the HeRo observational study. Surg Endosc. 2012; 26:3634–41. [PubMed: 22729704]

Lee LK, Whitehurst C, Chen Q, Patntelides ML, Hetzel FW, Moore J. Interstitial photodynamic therapy in the canine prostate. Br J Urol. 1997; 80:898–902. [PubMed: 9439405]

Kodama, LiL, Saito, KK., Aizawa, K. Phase-resolved fluorescence study of mono-L-aspartyl chlorin E6. J Photochem Photobiol B. 2002; 67:51–6. [PubMed: 12007467]

Liang X, Wang KK, Zhu TC. Singlet oxygen dosimetry modeling for photodynamic therapy. Proc SPIE. 2012; 8210:82100T-1-7.

Lin H, Shen Y, Chen D, Lin L, Wilson BC, Li B, Xie S. Feasibility Study on Quantitative Measurements of Singlet Oxygen Generation Using Singlet Oxygen Sensor Green. J Fluoresc. 2013; 23:41–7. [PubMed: 22914972]

Liu B, Farrell TJ, Patterson MS. Comparison of noninvasive photodynamic therapy dosimetry methods using a dynamic model of ALA-PDT of human skin. Phys Med Biol. 2012; 57:825–41. [PubMed: 22251621]

Liu B, Kim MM, Gallagher-Colombo SM, Busch TM, Zhu TC. Comparison of PDT parameters for RIF and H460 tumor models during HPPH-mediated PDT. Proc SPIE. 2014; 8931:89311C-1-6.

Liu B, Kim MM, Zhu TC. A theoretical comparison of macroscopic and microscopic modeling of singlet oxygen during Photfrin and HPPH-mediated PDT. Proc SPIE. 2013; 8568:856805.

Lovell JF, Liu TW, Chen J, Zheng G. Activatable Photosensitizers for imaging and therapy. Chem Rev. 2010; 110:2839–57. [PubMed: 20104890]

Lui H, Hobbs L, Tope WD, Lee PK, Elmets C, Provost N, Chan A, Neyndorff H, Y SX, Jain H, Hamzavi I, McLean D, Bissonnette R. Photodynamic therapy of multiple nonmelanoma skin cancers with verteporfin and red light-emitting diodes. Arch Dermatol. 2004; 140:26–32. [PubMed: 14732656]

Lustig RA, Vogl TJ, Fromm D, Cuenca R, Hsi RA, D'Cruz AK, Krajina Z, Turic M, Singhal A, Chen JC. A multicenter Phase I safety study of intratumoral photoactivation of talaporfin sodium in patients with refractory solid tumors. Cancer. 2003; 98:1767–71. [PubMed: 14534895]

Marks PV, Belchetz PE, Saxena A, Igbaseimokumo U, Thomson S, Nelson M, Stringer MR, Holroyd JA, Brown SB. Effect of photodynamic therapy on recurrent pituitary adenomas: clinical phase I/II trial - an early report. Br J Neurosurg. 2000; 14:317–25. [PubMed: 11045196]

Marti C, Nonell S, Nicolau M, Torres T. Photophysical Properties of Neutral and Cationic Tetrapyridinoporphyrazines. Phochem Photobiol. 2000; 71:53–9.

Mazor O, Brandis A, Plaks V, Neumark E, Rosenbach-Belkin V, Salomon Y, Scherz A. WST11, A Novel Water-soluble Bacteriochlorophyll Derivative; Cellular Uptake, Pharmacokinetics, Biodistribution and Vascular-targeted Photodynamic Activity Using Melanoma Tumors as a Model. Photochem Photobiol. 2005; 81:342–51. [PubMed: 15623318]

McCallum JEB, Kuniyoshi CY, Foote CS. Characterization of 5-hydroxy-8-oxo-7,8-dihydroguanosine in the photosensitized oxidation of 8-oxo-7,8-dihydroguanosine and its rearrangement to spiroiminodihydantoin. J Am Chem Soc. 2004; 126:16777–82. [PubMed: 15612716]

McDonagh AF. Phototherapy: From Ancient Egypt to the New Millennium. J Perinatol. 2001; 21:S7–S12. [PubMed: 11803408]

McMillan DD, Chen D, Kim MM, Liang X, Zhu TC. Parameter determination for singlet oxygen modeling of BPD-mediated PDT. Proc SPIE. 2013; 8568:856810.

Meng L, Wu Y, Yi T. A ratiometric fluorescent probe for the detection of hydroxyl radicals in living cells. Chem Commun. 2014; 50:4843–5.

Milanesio ME, Alvarez MG, Yslas EI, Borsarelli CD, Silber JJ, Rivarola V, Durantini EN. Photodynamic Studies of Metallo 5,10,15,20-Tetrakis(4-methoxyphenyl) porphyrin: Photochemical Characterization and Biological Consequences in a Human Carcinoma Cell Line. Photochem Photobiol. 2001; 74:14–21. [PubMed: 11460532]

Miller JD, Baron ED, Scull H, Hsia A, Berlin JC, McCormick T, Colussi V, Kenney ME, Cooper KD, Oleinick L. Photodynamic therapy with the phthalocyanine photosensitizer Pc 4: The case experience with preclinical mechanistic and early clinical-translational studies. Toxicol Appl Pharm. 2007; 224:290–9.

Mitra S, Foster TH. Photophysical Parameters, Photosensitizer Retention and Tissue Optical Properties Completely Account for the Higher Photodynamic Efficacy of meso-Tetra-Hydroxyphenyl-Chlorin vs Photofrin. Photochem Photobiol. 2005; 81:849–59. [PubMed: 15807635]

Moan J, Berg K. The photodegradation of porphyrins in cells can be used to estimate the lifetime of singlet oxygen. Photochem Photobiol. 1991; 53:549–53. [PubMed: 1830395]

Mody TD. Pharmaceutical development and medical applications of porphyrin-type macrocycles. J Porphyrins Phthalocyanines. 2000; 4:362–7.

Momma T, Hamblin MR, Wu HC, Hasan T. Photodynamic therapy of orthotopic prostate cancer with benzoporphyrin derivative: local control and distant metastasis. Cancer Res. 1998; 58:5425–31. [PubMed: 9850075]

Musbat L, Weitman H, Ehrenberg B. Azide Quenching of Singlet Oxygen in Suspensions of Microenvironments of Neutral and Surface Charged Liposomes and Micelles. Photochem Photobiol. 2013; 89:253–8. [PubMed: 22827592]

Nichols MG, Foster TH. Oxygen diffusion and reaction kinetics in the photodynamic therapy of multicell tumour speroids. Phys Med Biol. 1994; 39:2161–81. [PubMed: 15551546]

Niedre MJ, Patterson MS, Wilson BC. Direct Near-infrared Luminescence Detection of Singlet Oxygen Generated by Photodynamic Therapy in Cells In Vitro and Tissues In Vivo. Photochem Photobiol. 2002; 75:382–91. [PubMed: 12003128]

Nyokong T. Effects of substituents on the photochemical and photophysical properties of main group metal phthalocyanines. Coord Chem Rev. 2007; 251:1707–22.

Ogilby PR, Foote CS. Chemistry of singlet oxygen. 42. Effect of solvent, solvent isotopic substitution, and temperature on the lifetime of singlet molecular oxygen (1 Δ g). J Am Chem Soc. 1983; 105:3423–30.

Ohkubo K, Nanjo T, Fukuzumi S. Efficient photocatalytic oxygenation of aromatic alkene to 12-dioxetane with oxygen via electron transfer. Org Lett. 2005; 7:4265–8. [PubMed: 16146403]

Ohmori S, Arai T. In vitro behavior of Porfimer sodium and Talaporfin sodium with high intensity pulsed irradiation. Lasers Med Sci. 2006; 21:213–23. [PubMed: 17024319]

Ohmori S, Hakomori S, Arai T. Flow Rate and Fluence Rate Dependences of the Triplet-State Lifetime of Talaporfin Sodium Photochemical Reaction in Flowing Solution. Jpn J Appl Phys. 2007; 46:1217–9.

Ormond AB, S FH. Dye Sensitizers for Photodynamic Therapy. Materials. 2013; 6:817–40.

Ouedraogo GD, Redmond RW. Secondary Reactive Oxygen Species Extend the Range of Photosensitization Effects in Cells: DNA Damage Produced Via Initial Membrane Photosensitization. Photochem Photobiol. 2003; 77:192–203. [PubMed: 12785059]

Pandey RK, Sumlin AB, Constantine S, Aoudla M, Potter WR, Bellnier DA, Henderson BW, Rodgers MAJ, Smith KM, Dougherty TJ. Alkyl Ether Analogs of Chlorophyll-a Derivatives:Part 1. Synthesis, Photophysical Properties and Photodynamic Efficacy. Photochem Photobiol. 1996; 64:194–204. [PubMed: 8787014]

Patterson MS, Madsen SJ, Wilson BC. Experimental Tests of the Feasibility of Singlet Oxygen Luminescence Monitoring in vivo During Photodynamic Therapy. J Photochem Photobiol B. 1990; 5:69–84. [PubMed: 2111394]

Pedersen SK, Jolmehave J, Blaikie FH, Gollmer A, Breitenbach T, Jensen HH, Ogilby PR. Aarhus Sensor Green: A Fluorescent Probe for Singlet Oxygen. J Org Chem. 2014; 79:3079–87. [PubMed: 24605923]

Penjweini R, Kim MM, Zhu TC. In vivo outcome study of HPPH mediated PDT using singlet oxygen explicit dosimetry (SOED). Proc SPIE. 2015a; 9308:93080N-1-6.

Penjweini R, Liu B, Kim MM, Zhu TC. Explicit dosimetry for 2-(1-Hexyloxyethyl)-2-devinyl pyropheophorbide-a (HPPH) mediated photodynamic therapy: macroscopic singlet oxygen modeling. J Biomed Opt. 2015b; 20:128003-1-8. [PubMed: 26720883]

Plaetzer K, Krammer B, Berlanda J, Berr F, Kiesslich T. Photophysics and photochemistry of photodynamic therapy: fundamental aspects. Lasers Med Sci. 2009; 24:259–68. [PubMed: 18247081]

Pogue BW, Elliott JT, Kanick SC, Davis SC, Samkoe KS, Maytin EV, Pereira SP, Hasan T. Revisiting photodynamic therapy dosimetry: reductionist & surrogate approaches to facilitate clinical success. Phys Med Biol. 2016; 61:R57–R89. [PubMed: 26961864]

Poole DC, Behnke BJ, McDonough P, McAllister RM, Wilson DF. Measurement of muscle microvascular oxygen pressures: Compartmentalization of phosphorescent probe. Microcirculation. 2004; 11:317–26. [PubMed: 15280071]

Pouget JP, Douki T, Richard MJ, Cadet J. DNA damage induced by cells by γ and UVA Radiation as Measured by HPLC/GC-MS and HPLC-EC and Comet Assay. Chem Res Toxicol. 2000; 13:541–9. [PubMed: 10898585]

Price M, Heilbrun L, Kessel D. Effects of the Oxygenation level on Formation of Different Reactive Oxygen Species During Photodynamic Therapy. Photochem Photobiol. 2013; 89:683–6. [PubMed: 23216021]

Price M, Reiners JJ, Santiago AM, Kessel D. Monitoring Singlet Oxygen and Hydroxyl Radical Formation with Fluorescent Probes During Photodynamic Therapy. Photochem Photobiol. 2009; 85:1177–81. [PubMed: 19508643]

Qiu H, Kim MM, Penjweini R, Zhu TC. Dosimetry study of PHOTOFRIN-mediated photodynamic therapy in a mouse tumor model. Proc SPIE. 2016; 9694:96940T-1–7.

Ragas X, Jimenez-Banzo A, Sanchez-Garcia D, Batllori X, Nonell S. Singlet oxygen photosensitisation by the fluorescent probe Singlet Oxygen Sensor Green®. Chem Commun. 2009; 20:2920–2.

Ranby B. The History of Singlet Oxygen - An Introduction. Kem Tidskr. 1981; 93:36–7.

Redmond RW, Gamlin J. A Compilation of Singlet Oxygen Yields from Biologically Relevant Molecules. Photochem Photobiol. 1999; 70:391–475. [PubMed: 10546544]

Robinson DJ, de Bruijn HS, van der Veen N, Stringer MR, Brown SB, Star WM. Fluorescence Photobleaching of ALA-induced Protoporphyrin IX during Photodynamic Therapy of Normal Hairless Mouse Skin: The Effect of Light Dose and Irradiance and the Resulting Biological Effect. Photochem Photobiol. 1998; 67:140–9. [PubMed: 9477772]

Rodgers MAJ, Lee PC. Singlet Molecular Oxygen in Micellar Systems. 2. Quenching Behavior in AOT Reverse Micelles. J Phys Chem. 1984; 88:3480–4.

Russell JA, Diamond KR, Collins TJ, Tiedje HF, Hayward JE, Farrell TJ, Patterson MS, Fang Q. Characterization of Fluorescence Lifetime of Photofrin and Delta-Aminolevulinic Acid Induced Protoporphyrin IX in Living Cells Using Single- and Two-Photon Excitation. IEEE J Sel Top Quant Electron. 2008; 14:158–66.

S AJ, Browne RJ, Ogryzlo EA. The red emission bands of molecular oxygen. Photochem Photobiol. 1965; 4:963–9.

Setsukinai K, Urano Y, Kakinuma K, Majima HJ, Nagano T. Development of Novel Fluorescence Probes That Can Reliably Detect Reactive Oxygen Species and Distinguish Specific Species. J Biol Chem. 2003; 278:3170–5. [PubMed: 12419811]

Sharman WM, Allen CM, van Lier JE. Role of activated oxygen species in photodynamic therapy. Method Enzymol. 2000; 319:376–400.

Sheu C, Foote CS. Endoperoxide formation in a guanosine derivative. J Am Chem Soc. 1993; 115:10446–7.

Shonat RD, Kight AC. Oxygen tension imaging in the mouse retina. Ann Biomed Eng. 2003; 31:1084–96. [PubMed: 14582611]

Simone CB, Friedberg JS, Glatstein E, Stevenson JP, Sterman DH, Hahn SM, Cengel KA. Photodynamic therapy for the treatment of non-small cell lung cancer. J Thorac Dis. 2012; 4:63–75. [PubMed: 22295169]

Spikes JD, Bommer JC. Photobleaching of mono-L-aspartyl chlorine e6 (NPe6): a candidate sensitizer for the photodynamic therapy of tumors. Photochem Photobiol. 1993a; 58:346–50. [PubMed: 8234467]

Spikes JD, Bommer JC. Photosensitizing properties of mono-L-aspartyl chlorin e6 (NPe6): a candidate sensitizer for the photodynamic therapy of tumors. J Photochem Photobiol B. 1993b; 17:135–43. [PubMed: 8459317]

Sporn LA, Foster TH. Photofrin and Light Induces Microtubule Depolymerization in Cultured Human Endothelial Cells. Cancer Res. 1992; 52:3443–8. [PubMed: 1534512]

Sterenborg HJCM, van Gemert MJC. Photodynamic therapy with pulsed light sources: a theoretical analysis. Phys Med Biol. 1996; 41:835–49. [PubMed: 8735252]

Strickler SJ, Berg RA. Relationship between abosorption intensity and fluorescence lifetime of molecules. J Chem Phys. 1962; 37:814–22.

Stripp DCH, Mick R, Zhu TC, Whittington R, Smith D, Dimofte A, Finlay JC, Miles J, Busch TM, Shin D, Kachur A, Tochner ZA, Malkowicz SB, Glatstein E, Hahn SM. Phase I trial of motexafin-lutetium-mediated interstitial photodynamic therapy in patients with locally recurrent prostate cancer. Proc SPIE. 2004; 5315:88–99.

Touma D, Yarr M, Whitehead S, Konnikov N, Gilchrest BA. A trial of short incubation, broad-area photodynamic therapy for facial actinic keratoses and diffuse photodamage. Arch Dermatol. 2004; 40:33–40.

Turro, NJ., Ramamurthy, V., Scaiano, JC. Modern Molecular Photochemistry of Organic Molecules. Sausalito, CA: University Science Book; 2010.

Vakrat-Haglili Y, Weiner L, Brumfeld V, Brandis A, Salomon Y, McIlroy B, Wilson BC, Pawlak A, Rozanowska M, Sarna T, Scherz A. The Microenvironment Effect on the Generation of Reactive Oxygen Species by Pd-Bacteriopheophorbide. J Am Chem Soc. 2005; 127:6487–97. [PubMed: 15853357]

Verigos K, Stripp DCH, Mick R, Zhu TC, Whittington R, Smith D, Dimofte A, Finlay J, Busch TM, Tochner ZA, Malkowicz SB, Glatstein E, Hahn SM. Updated Results of a Phase I Trial of Motexafin Lutetium-Mediated Interstitial Photodynamic Therapy in Patients with Locally Recurrent Prostate Cancer. J Environ Pathol Toxicol Oncol. 2006; 25:373–88. [PubMed: 16566729]

Walsh A. The application of atomic absorption spectra to chemical analysis. Spectrochim A. 1955; 7:108–17.

Wang KK, Finlay Jc, Busch Tm, Hahn Sm, Zhu TC. Explicit dosimetry for photodynamic therapy: macroscopic singlet oxygen modeling. J Biophoton. 2010; 3:304–18.

Wang KK, Mitra S, Foster TH. A comprehensive mathematical model of microscopic dose deposition in photodynamic therapy. Med Phys. 2007; 34:282–93. [PubMed: 17278514]

Wasserman, Hh. Singlet Oxygen. New York, New York: Academic Press Inc; 1979.

Wasserman, Hh, Larsen, DL. Formation of 14-endoperoxides from the dye-sensitized photo-oxygenation of alkylnaphthalenes. J Chem Soc Chem Commun. 1972:253–4.

Weersink RA, Bogaards A, Gertner M, Davidson SRH, Zhang K, Netchev G, Trachtenberg J, Wilson Bc. Techniques for delivery and monitoring of TOOKAD (WST09)-mediated photodynamic therapy of the prostate: Clinical experience and practicalities. J Photochem Photobiol B. 2005a; 79:211–22. [PubMed: 15896648]

Weersink RA, Forbes J, Bisland S, Trachtenberg J, Elhilali M, Brun Ph, Wilson BC. Assesment of Cutaneous Photosensitivity of TOOKAD (WST09) in Preclinical Animal Models and in Patients. Photochem Photobiol. 2005b; 81:106–13. [PubMed: 15382963]

Weishaupt KR, Gomer CJ, Dougherty TJ. Identification of singlet oxygen as the cytotoxic agent in photo-activation of a murine tumor. Can Res. 1976; 36:2326–92.

Weldon D, Poulsen Td, Mikkelsen Kv, Ogilby PR. Singlet Sigma: The "Other" Singlet Oxygen in Solution. Photochem Photobiol. 1999; 70:369–79.

Wessels, Jm, Rodgers, MAJ. Detection of the O2(l Δ g)-O2(3 Σ g-1) transition in Aqueous Environments: A Fourier-transform near-infrared luminescence study. J Phys Chem. 1995; 99:15725–7.

Weston, Ma, Patterson, MS. Calculation of Singlet Oxygen Dose Using Explicit and Implicit Dose Metrics During Benzoporphyrin Derivative Monoacid Ring A (BPD-MA)-PDT In Vitro and Correlation with MLL Cell Survival. Photochem Photobiol. 2011; 87:1129–37. [PubMed: 21575000]

Wezgowiec J, Derylo MB, Teissie J, Orio J, Rols MP, Kulbacka J, Saczko J, Kotulska M. Electric Field-Assisted Delivery of Photofrin to Human Breast Carcinoma Cells. J Membrane Biol. 2013; 246:725–35. [PubMed: 23546012]

Wiedmann M, Berr F, Schiefke I, Witzigmann H, Kohlhaw K, Mossner J, Caca K. Photodynamic therapy in patients with non-resectable hilar cholangiocarcinoma: 5-year follow-up of a prospective phase II study. Gastrointest Endosc. 2004; 60:68–75. [PubMed: 15229428]

Wiedmann M, Caca K, Berr F, Schiefke I, Tannapfel A, Wittekind C, Mossner J, Hauss J, Witzigmann H. Neoadjuvant photodynamic therapy as a new approach to treating hilar cholangiocarcinoma: a phase II pilot study. Cancer. 2003; 97:2783–90. [PubMed: 12767091]

Wilkinson F, Brummer JG. Rate Constants for the Decay and Reactions of the Lowest Electronically Excited Singlet State of Molecular Oxygen in Solution. J Phys Chem Ref Data. 1981; 10:809–999.

Wilkinson F, Helman Wp, Ross AB. Quantum yields for the photosensitized formation of the lowest electronically excited singlet state of molecular oxygen in solution. J Phys Chem Ref Data. 1993; 22:113–262.

Wilson, Bc, Patterson, MS. The physics, Biophysics, and technology of photodynamic therapy. Phys Med Biol. 2008; 53:R61–109. [PubMed: 18401068]

Yapici NB, Jockusch S, Moscatelli A, Mandalapu SR, Itagaki Y, Bates Dk, Weiseman S, Gibson Km, Turro NJ, Bi L. New Rhodamine Nitroxide Based Fluorescent Probes for Intracellular Hydroxyl Radical Identification in Living Cells. Org Lett. 2012; 14:50–3. [PubMed: 22176578]

Yuan L, Lin W, Song J. Ratiometric fluorescent detection of intracellular hydroxyl radicals based on a hybrid coumarin–cyanine platform. Chem Commun. 2010; 46:7930–2.

Zaklika KA, Thayer AL, Schaap A. Substituent effects on the decomposition of 1,2-dioxetanes. J Am Chem Soc. 1978; 100:4916–8.

Zamadar, M., Greer, A. Handbook of Synthetic Photochemistry. Albini, A., Fagnoni, M., editors. Weinheim: John Wiley & Sons; 2010. p. 353-86.

Zhao B, Yin J, Bilski Pj, Chignell Cf, Roberts Je, He Y. Enhanced photodynamic efficacy towards melanoma cells by encapsulation of Pc4 in silica nanoparticles. Toxicol Appl Pharm. 2009; 241:163–72.

Zhu, Tc, Finlay, JC. The role of photodynamic therapy (PDT) Physics. Med Phys. 2008; 35:3127–36.

Zhu TC, Finlay JC, Hahn SM. Determination of the distribution of light, optical properties, drug concentration, and tissue oxygenation in-vivo in human prostate during motexafin lutetium-mediated photodynamic therapy. Photochem Photobiol. 2005; 79:231–41.

Zhu TC, Finlay JC, Zhou X, Li J. Macroscopic modeling of the singlet oxygen production during PDT. Proc SPIE. 2007; 6427:1–12.

Zhu TC, Hahn Sm, Kapatkin As, Dimofte A, Rodriquez Ce, Vulcan Tg, Glatstein E, Hsi Ra. In vivo Optical Properties of Normal Canine Prostate at 732 nm Using Motexafin Lutetium-mediated Photdynamic Therapy. Photochem Photobiol. 2003; 77:81–8. [PubMed: 12856887]

Zhu TC, Kim Mm, Liang X, Finlay Jc, Busch TM. In-vivo singlet oxygen threshold doses for PDT. Photon Lasers Med. 2015a; 4:59–71.

Zhu, Tc, Li, B., Kim, MM. Computer models of the dynamic processes in photodynamic therapy. In: Zhang, G., editor. Computational Bioengineering. CRC Taylor & Francis); 2015b. p. 231-64.

Zhu, TC., Liu, B. Singlet Oxygen Modeling of PDT incorporating Local Vascular Oxygen Diffusion; Proc COMSOL User Conference; 2013. p. 1-4.

Zhu TC, Liu B, Kim Mm, McMillan DD, Liang X, Finlay Jc, Busch TM. Comparison of singlet oxygen threshold doses for PDT. Proc SPIE. 2014; 8931:89310I-1–10.

Zhu TC, Liu B, Penjweini R. Study of tissue oxygen supply rate in a macroscopic photodynamic therapy singlet oxygen model. J Biomed Opt. 2015c; 20:038001–1-13. [PubMed: 25741665]

List of Symbols

α $^3O_2$ solubility coefficient, see Eq. B3 (μM mmHg^{-1})

α_c $^3O_2$ solubility in plasma, see Eq. B1 (μM mmHg^{-1})

α_t $^3O_2$ solubility in tissue, see Eq. B4 (μM mmHg^{-1})

β $(k_4 + k_8 [A])/k_2$, see Table 2, (μM)

Γ rate of the oxygen loading/unloading, see Eq. 17 (μM s^{-1})

δ low concentration correction, see Table 2, Eq. 18 (μM)

ε extinction coefficient, see Table 2, Eq. 19, (cm$^{-1}\mu$M^{-1})

η Hypoxic reaction consumption rate, see Table 2 (cm^{2}mW^{-1}s$^{-1}\mu$M)

ξ Specific oxygen consumption rate, see Table 2, (cm^{2}mW^{-1}s^{-1})

σ Specific photobleaching ratio, see Table 2, (μM^{-1})

τ_f fluorescence lifetime, see Table 2, (s)

τ_t triplet lifetime, see Table 2, (s)

τ_Δ singlet oxygen lifetime, see Table 2, (s)

ϕ fluence rate, see Eq. 19, (mW cm^{-2})

Φ_f fluorescence quantum yield, see Table 2

Φ_t triplet quantum yield, see Table 2

Φ_Δ singlet oxygen quantum yield, see Table 2

Φ_{ROS}	superoxide anion quantum yield, see Table 2
$[A]$	biological substrates that are singlet oxygen receptors, see Table 2, Eq. 10 (μM)
C_H	Hemoglobin concentration in blood, see Eq. B2 (μM)
D_c	$^3O_2$ diffusion coefficient in capillary, see Eq. B1 (μm^{2}s^{-1})
D_H	Hemoglobin diffusion coefficient, see Eq. B2 (μm^{2}s^{-1})
D_s	$^3O_2$ diffusion coefficient in vascular media, see Eq. B5 (μm^{2}s^{-1})
D_t	$^3O_2$ diffusion coefficient in tissue, see Eq. B4 (μm^{2}s^{-1})
g	oxygen perfusion rate, see Table 2, Eq. 17 (μM s^{-1})
k_0, k_a	photon absorption rate of photosensitizer per photosensitizer concentration, $k_0 \varepsilon \phi / h v$, see Table 1, Eq. 1 (s^{-1})
k_1, k_{os}	bimolecular rate for $^1O_2$ reaction with ground-state photosensitizer, see Table 1, Eq. 2 (μM^{-1}s^{-1})
k_2, k_{ot}	bimolecular rate of triplet photosensitizer quenching by $^3O_2$, see Table 1, Eq. 3 (μM^{-1}s^{-1})
k_3, k_f	decay rate of first excited singlet state photosensitizer to ground state photosensitizer, k_3 k $_{3NR} + k_{3R}$, see Table 1, Eq. 1 (s^{-1})
k_{3NR}	non-radiative (spontaneous) decay rate of first excited singlet state photosensitizer to ground state photosensitizer, see Table 2, Eq. 1 (s^{-1})
k_{3R}	radiative (fluorescence) rate of monomolecular decay of the first excited singlet state photosensitizer to ground state photosensitizer, see Eq. 1 (s^{-1})
k_4, k_p	phosphorescence decay rate of the photosensitizer triplet state to ground state, k_4 $k_{4NR} + k_{4R}$, see Table 1, Eq. 5 (s^{-1})
k_{4NR}	non-radiative rate of monomolecular decay of the photosensitizer triplet state, see Eq. 42 (s^{-1})
k_{4R}	radiative rate of monomolecular decay of the photosensitizer triplet state, see Eq.42 (s^{-1})
k_5, k_{isc}	intersystem crossing rate of first excited photosensitizer to triplet state photosensitizer, see Table 1, Eq. 6 (s^{-1})
k_6, k_d	$^1O_2$ to $^3O_2$ phosphorescence decay rate, see Table 1, Eq. 13 (s^{-1})
k_7, k_{oa}	bimolecular rate of reaction of $^1O_2$ with biological substrate $[A]$, see Table 1, eq 14 (μM^{-1}s^{-1})
k_8, k_{ta}	bimolecular rate of reaction of T$_1$ with biological substrate $[A]$, see Table 1, Eq. 8 (μM^{-1}s^{-1})

k_q	physical quenching rate of $^1O_2$ by substrate *[A]*, see Eq. 9, (s^{-1})
k_r	chemical quenching rate of $^1O_2$ by substrate *[A]*, see Eq. 9, (s^{-1})
P	Oxygen partial pressure, see Eq. B3 (mmHg)
P_m	Oxygen partial pressure at half maximum oxygen consumption concentration, see Eq. B3 (mmHg)
q_0	$^3O_2$ maximum metabolic consumption rate, see Eq. B4, ($\mu M\ s^{-1}$)
S	Fraction of triplet state photosensitizer reactions that are non-luminescent, see Table 2
S_Δ	fraction of triplet-state photosensitizer-$^3O_2$ reactions to produce $^1O_2$, see Table 2
S_I	fraction of triplet state photosensitizer-$^3O_2$ reactions that involve type I reactions, see Table 2
S_0	photosensitizer in its ground state, see fig. 2
S_1	photosensitizer in its first singlet state, see fig. 2
$Sa\ (SaO_2)$	hemoglobin oxygen saturation, see Eq. B2
T_1	photosensitizer in its first triplet state, see fig. 2
v	velocity of blood flow, see Eq. B1, B2 ($\mu m\ s^{-1}$)
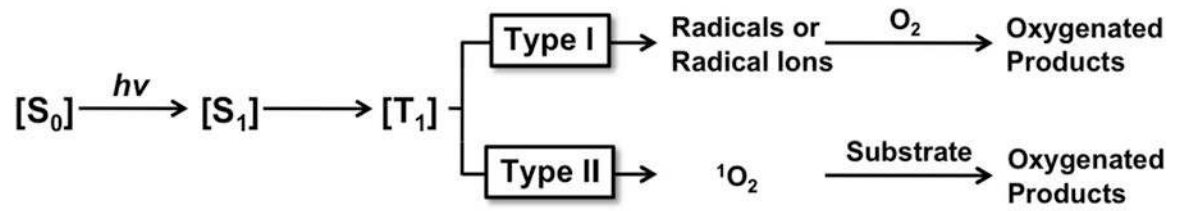
Figure 1.
Type I and type II photosensitized oxidations. The type I pathway produces radicals or
radical ions, which in subsequent reactions produces ROS. The type II pathway is primarily
due to energy transfer from an excited photosensitizer to triplet oxygen to produce singlet
oxygen.
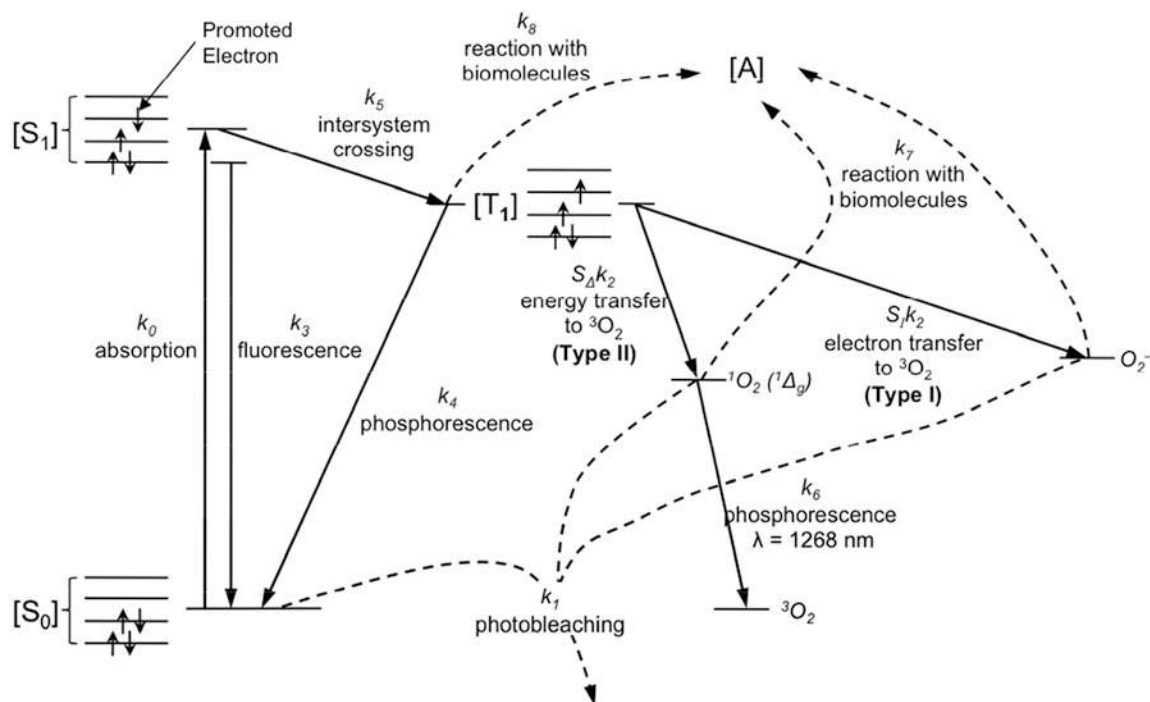
Figure 2.
Diagram for the photoactivation of photosensitizer in the presence of oxygen and biomolecules. The photosensitizer in its ground state (S_0) absorbs a photon and is excited to its first singlet state (S_1). It spontaneously decays to its excited triplet state (T_1) via intersystem crossing (ISC). From T_1, energy is transferred to ground state molecular oxygen ($^3O_2$), creating reactive singlet oxygen ($^1O_2$) for a typical type II reaction. In type I reactions, the triplet photosensitizer will transfer an electron to $^3O_2$ which reacts with molecular targets to produce radical species, or less common interact directly with the acceptor, [A], without oxygen mediation. k_3 and $k_{4\_}$ include both radiative and non-radiative decay rates for fluorescence and phosphorescence, respectively (see Table 1).
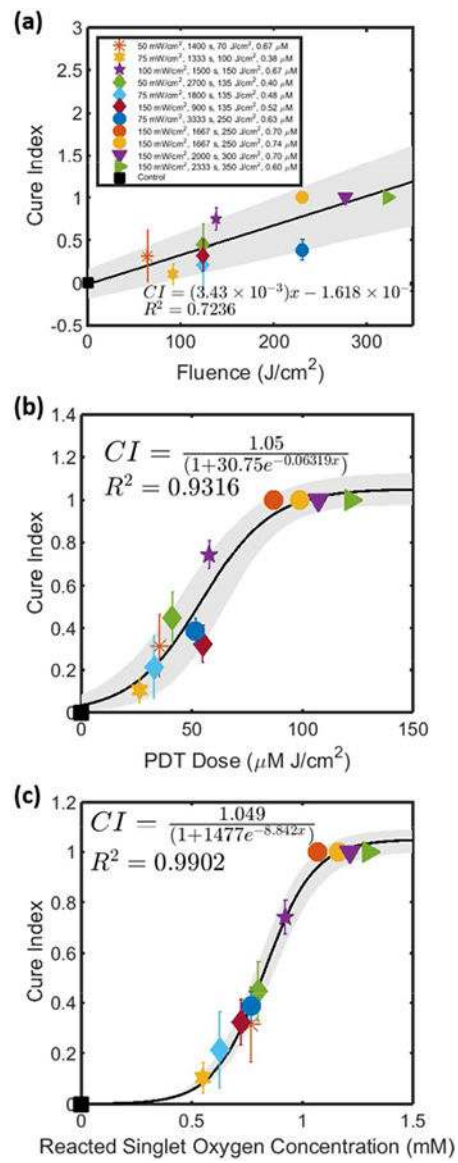
Figure 3.
Cure index vs. (a) light fluence (b) PDT dose and (c) calculated reacted singlet oxygen for BPD mediated PDT in RIF tumor. The grey regions indicate the 95% confidence intervals of the fitted line (in black). The goodness of the fit, R^2, is also shown.

Secondary (Photochemical) Reactions

$$O_2^{-\bullet} + H_2O \rightleftharpoons HO_2^{\bullet} + OH^{-\bullet}$$

$$O_2^{-\bullet} + O_2^{-\bullet} \longrightarrow H_2O_2$$

$$O_2^{-\bullet} + H_2O_2 \longrightarrow O_2(^3\Sigma_g^-) + OH^- + OH^{-\bullet}$$

$$O_2^{-\bullet} + Fe(III) \longrightarrow {}^3O_2(^3\Sigma_g^-) + Fe(II)$$

$$Fe(II) + H_2O_2 \longrightarrow Fe(III) + OH^- + OH^{-\bullet}$$

Cytotoxic Reactions

$OH^{-\bullet}$
H_2O_2 $\longrightarrow$ Oxidation of Acceptors $\longrightarrow$ Cellular Damage
$O_2^{-\bullet}$
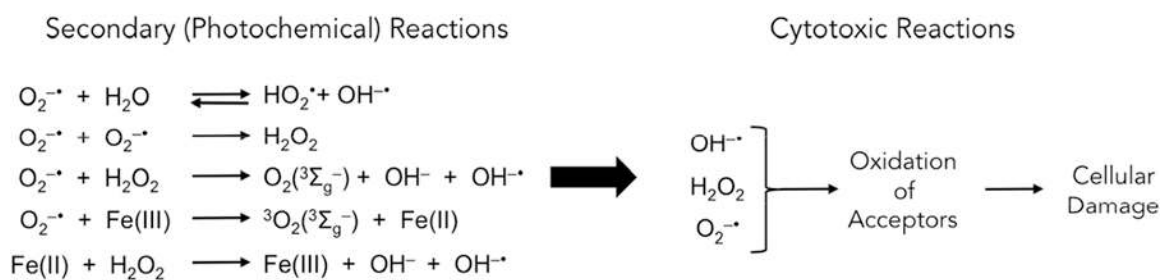
Figure 4.

Secondary (photochemical) reactions for type I photosensitizer to generate the resulting reactive oxygen species (HO, H_2O_2, $O_2-\cdot$) Other redox active metals are also pertinent for generation of ROS and should be included as part of secondary reactions in "…". ROS will in turn oxidate acceptors in cells to cause cellular damage.
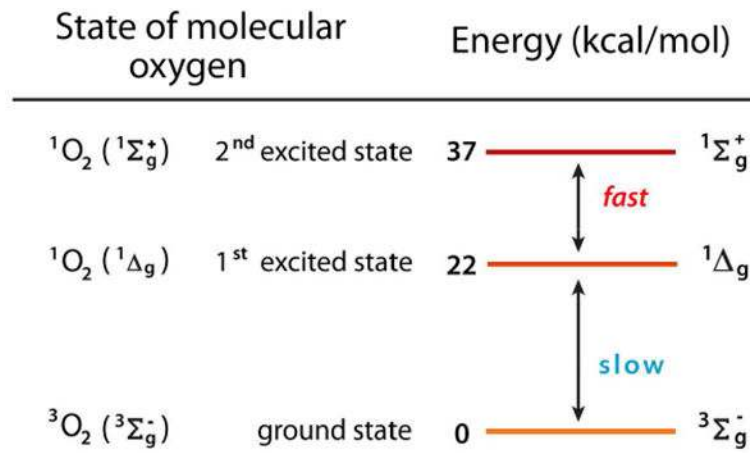
Figure 5.
Energy diagram of triplet ground-state O_2 ($^3\Sigma_g^-$), excited singlet delta ($^1\Delta_g$) and excited singlet sigma ($^1\Sigma_g^+$) state of oxygen.
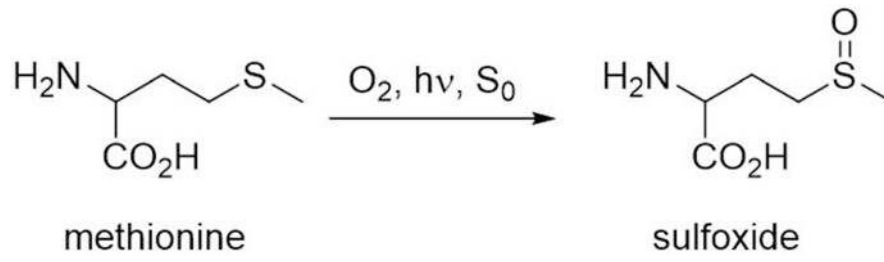
Figure 6.
Reaction of methionine with $^1O_2$ to form sulfoxide. S_0 = photosensitizer and CH_2Cl_2 = dichloromethane solvent.
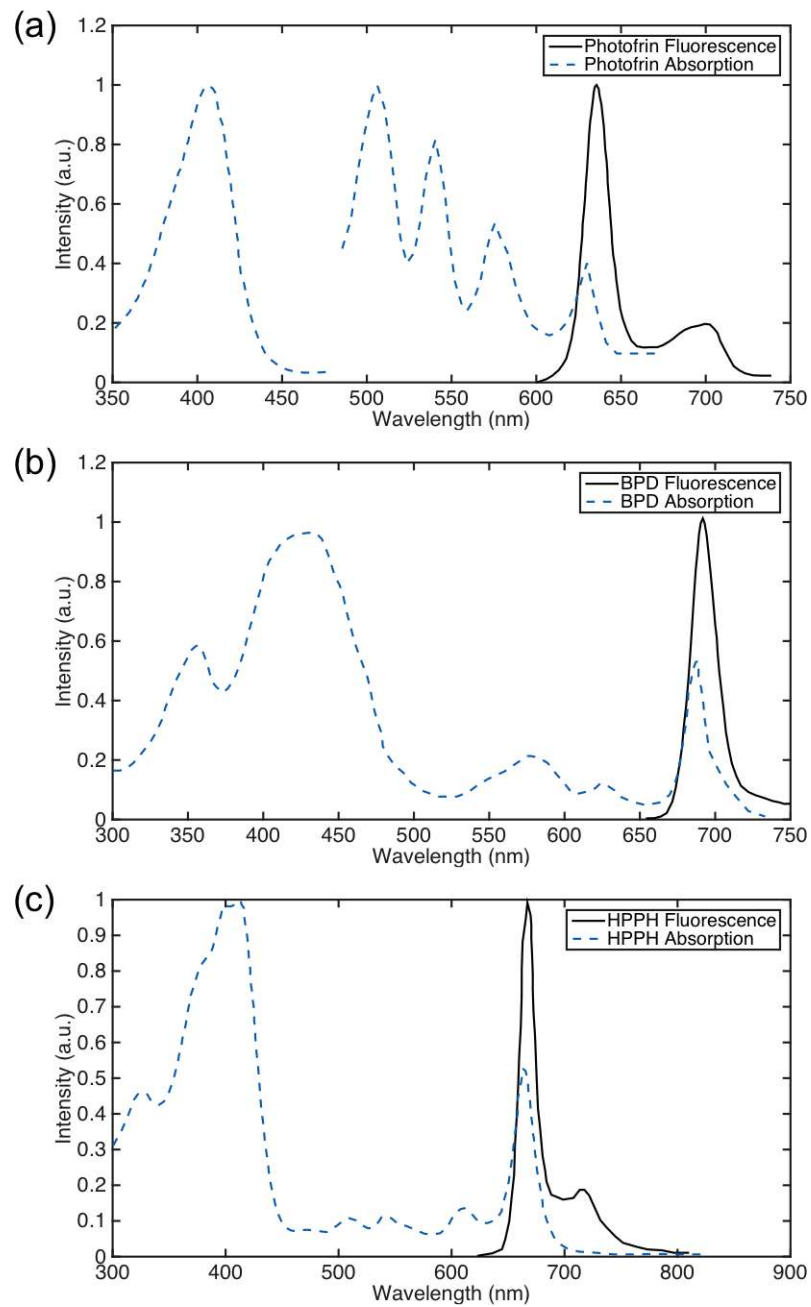
Figure 7.
Fluorescence spectra (solid line) and absorption spectra (dashed line) of (a) Photofrin in PBS, (b) BPD in PBS, and (c) HPPH in water. Spectra are taken from (Wezgowiec *et al.*, 2013), (Aveline *et al.*, 1994), and (Kim *et al.*, 2007) with permission.

Table 1

Definition of photochemical reaction rate constants.

Symbol*	Definition
k_0, k_a (s^{-1})	Photon absorption rate of photosensitizer as a function of photosensitizer concentration (in μM), $k_0 = \varepsilon\phi/h\nu$, for ϕ=100 mW/cm^2.
k_1, k_{os} (μM^{-1}s^{-1})	Bimolecular decay rate for $^1O_2$ (k_{12}) and ROS (k_{11}) reactions with ground-state photosensitizer
k_2, k_{ot} (μM^{-1}s^{-1})	Bimolecular decay rate of triplet photosensitizer quenching by $^3O_2$
	$S_I k_2$ Reactions involving triplet state and electron transfer to $^3O_2$ (type I)
	$S_\Delta k_2$ Reactions involving triplet state and energy transfer to $^3O_2$ (type II)
k_3, k_f (s^{-1})	Fluorescence decay rate of first excited singlet state photosensitizer to ground state photosensitizer including internal conversion (non-radiative, k_{3NR}) and fluorescent (radiative, k_{3R}) terms
k_4, k_p (s^{-1})	Phosphorescence decay of the photosensitizer triplet state to ground state photosensitizer, including radiative (k_{4R}) and non-radiative (k_{4NR}) components
k_5, k_{isc} (s^{-1})	Intersystem crossing (ISC) decay rate from first excited photosensitizer to triplet state photosensitizer
k_6, k_d (s^{-1})	Phosphorescence (or luminescence) decay rate of $^1O_2$ to $^3O_2$
k_7, k_{oa} (μM^{-1}s^{-1})	Bimolecular decay rate of reaction of type II $^1O_2$ (k_{72}) and type I ROS (k_{71}) with biological substrate [A]
k_8, k_{ta} (μM^{-1}s^{-1})	Bimolecular decay rate constant for reaction of triplet photosensitizer with substrate [A] for type I reactions

*
The first symbol is used in this paper. The second symbol is also commonly found in the literature
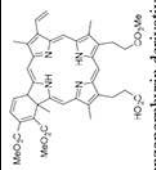
Table 2

Definition of some key parameters used in PDT modeling.
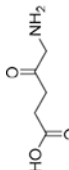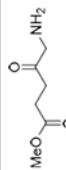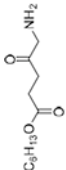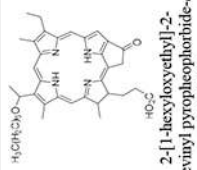
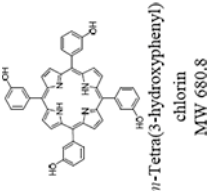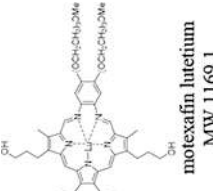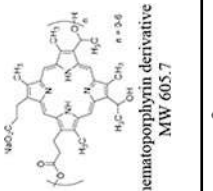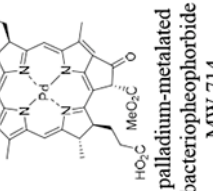| Symbol	Definition
β (μM)	Oxygen quenching threshold concentration $\dfrac{k_4 + k_g[A]}{k_2}$
δ (μM)	Low concentration correction
η (cm²mW⁻¹s⁻¹μM)	Hypoxic reaction consumption rate $\Phi_t \dfrac{\varepsilon}{h\nu} \dfrac{k_8[A]}{k_2}$
ξ (cm²mW⁻¹s⁻¹)	Specific oxygen consumption rate $\xi = \xi_{II} + \xi_I = S_\Delta \Phi_t \dfrac{\varepsilon}{h\nu} + S_I \Phi_t \dfrac{\varepsilon}{h\nu}$
σ (μM⁻¹)	Specific photobleaching ratio $\sigma = (\xi_{II}\sigma_{II} + \xi_I\sigma_I)/\xi$ where $\sigma_{II} = k_{12}\tau_\Delta$ and $\sigma_I = k_{11}\tau_s$
g (μM/s)	Macroscopic maximum oxygen supply rate
e (cm⁻¹μM⁻¹)	Photosensitizer extinction coefficient
τ_f (s)	Fluorescence lifetime $\dfrac{1}{k_3 + k_5}$
τ_Δ (s)	Singlet oxygen lifetime $\dfrac{1}{k_{12}([S_0] + \delta) + k_6 + k_{72}[A]}$
τ_s (s)	Superoxide (ROS) lifetime $\dfrac{1}{k_{11}([S_0] + \delta) + k_{71}[A]}$
τ_t (s)	Triplet state lifetime $\dfrac{1}{k_4 + k_2[^3O_2] + k_8[A]}$
$[A]$ (μM)	Singlet oxygen receptors, considered a constant during PDT because it is too large to be changed during PDT.
S_Δ	Fraction of triplet-state photosensitizer-³O₂ reactions to produce ¹O₂
S_I	Fraction of triplet-state photosensitizer reactions involved in Type I reactions
S_{NL}	Fraction of triplet state photosensitizer reactions that are non-luminescent $S_\Delta + S_I + S_{NL} = 1$
Φ_Δ	Singlet oxygen quantum yield $S_\Delta \dfrac{k_5}{k_3 + k_5}$
φ_{ROS}	Superoxide anion quantum yield $S_1 \dfrac{k_5}{k_3 + k_5}$
Φ_f	Fluorescence quantum yield $\dfrac{k_3}{k_3 + k_5} \dfrac{k_{3R}}{k_3}$ where k_{3R} is fluorescence radiative decay rate between S_1 and S_0
Φ_t	Triplet quantum yield $\dfrac{k_5}{k_3 + k_5}$

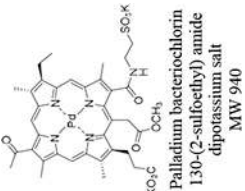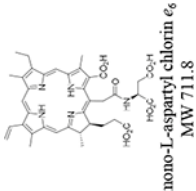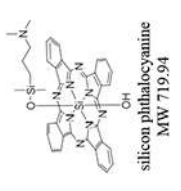**Table 3**

Summary of the experimental methods described in this section

Method			References
Direct Methods	Continuous Wave	Transient/Lifetime	
Absorption	Absorption spectroscopy (k_0, e) (*in-vivo/in-vitro*)	Transient absorption spectroscopy (Φ_Δ (*in-vitro* mostly)	(Fuwa and Valle, 1963; Walsh, 1955; Aveline *et al.*, 1998; Chattopadhyay *et al.*, 1984; Krieg and Redmond, 1993; Krieg *et al.*, 1993b)
Fluorescence	Fluorescence spectroscopy ([S_0]) (*in-vivo/in-vitro*)	FLI, FLIM (τ_f, k_3, k_5) (*in-vitro* mostly)	(Finlay *et al.*, 2001; Kress *et al.*, 2003; Lakowicz *et al.*, 1992)
Phosphorescence	Phosphorescence spectroscopy	LIOAC (Φ_t) SOL detection (τ_t, τ_Δ, k_1, k_2, k_4, k_6, k_7) (*in-vitro* mostly) Phosphorescence spectroscopy ([$^3O_2$]) (*in-vivo/in-vitro*)	(Aveline *et al.*, 1994) (Celaje *et al.*, 2011; Clennan *et al.*,1995; Hirano *et al.*, 2002; Hurst *et al.*, 1982; Jarvi *et al.*, 2006; Jensen *et al.*, 2010; Kanofsky, 1990; Khan and Kasha, 1963, 1964, 1970, 1979; Krasnovskii, 1976; Kress *et al.*, 2003; Marti *et al.*, 2000; Niedre *et al.*, 2002; Ogilby and Foote, 1983; Poole *et al.*, 2004; S. *et al.*, 1965; Shonat and Kight, 2003; Wessels and Rodgers, 1995; Wilkinson *et al.* 1993)
Indirect Methods			
SOED	*In-vitro* studies (ξ, σ, β, δ)		(Dysart and Patterson, 2006; Foster *et al.*, 1993; Foster *et al.*, 1991; Georgakoudi *et al.*, 1997; Nichols and Foster, 1994; Patterson *et al.*, 1990)
	In-vivo studies (ξ, σ, β, δ, g)		(Kim *et al.*, 2015a; Kim *et al.*, 2014a; Kim *et al.*, 2015b; Liang *et al.*, 2012; Liu *et al.*, 2014; Liu *et al.*, 2013; McMillan *et al.*, 2013; Penjweini *et al.*, 2015a; Wang *et al.*, 2010; Zhu *et al.*, 2007; Zhu *et al.*, 2015a; Zhu and Liu, 2013; Zhu *et al.*, 2014)
Other Methods			
	Singlet oxygen trapping ([$^1O_2$])		(Ohkubo *et al.*, 2005; Kotani *et al.*, 2004; Kim *et al.*, 2014b; Pedersen *et al.*, 2014; Ragas *et al.*, 2009)
	NMR spectroscopy ([$^1O_2$])		(Baumstark, 1988a)
	SOSG ([$^1O2$], Φ_Δ)		(Lin *et al.*, 2013)
	APF, HPF ([HO·])		(Setsukinai *et al.*, 2003)

Table 4

Characteristics of common photosensitizers and their FDA status.

Photosensitizer (trade name)	Chemical Structure	Approval	λ_{ex} (nm)	DLI $[1]$ (h)	Clearance Time	References
ALA-PpIX (Levulan, Alacare, Ameluz, Gliolan(for photodiagnosis))	5-aminolevulinic acid MW 131.1	1999 (FDA) 2009 2011 2007 (EMA)	405, 635	14-18	~2 days	(Ericson et al., 2004; Hage et al., 2004; Kelty et al., 2004; Touma et al., 2004)
Methyl ALA-PpIX (Medvix, Metvixia)	methyl aminolevulinate MW 145.2	2004 (FDA)	405, 635	3	~2 days	(Dragieva et al., 2004)
Hexyl ALA-PpIX (Hexvix)	hexyl-5-aminolevulinate MW 215.3		405	1-3	~2 days	(Krammer and Plaetzer, 2008)
BPD-MA (Verteporfin, Visudyne)	benzoporphyrin derivative monoacid ring A MW 718.8	2000 (FDA)	689	0.25- 3	5 days	(Chen et al., 2005; Momma et al., 1998; Lui et al., 2004; Azab et al., 2005)
HPPH	2-[1-hexyloxyethyl]-2-devinyl pyropheophorbide-α MW 636.8		665	24	~3 days	(Bellnier et al., 2003)

Photosensitizer (trade name)	Chemical Structure	Approval	λ_{ex} (nm)	DLI [11] (h)	Clearance Time	References
mTHPC (Foscan)	m-Tetra(3-hydroxyphenyl) chlorin MW 680.8	2001 (EMA)	652	48-110	15 days	(Verigos et al., 2006)
mLu (Lu-Tex)	motexafin lutetium MW 1169.1		732	3	~2 days	(Verigos et al., 2006; Stripp et al., 2004)
Porfimer sodium (Photofrin)	hematoporphyrin derivative MW 605.7	1998, 2003 (FDA) 2004 (EMA)	630	48-150	4-6 weeks	(Cuenca et al., 2004; Wiedmann et al., 2003; Wiedmann et al., 2004; Marks et al., 2000; Igbaseimokumo, 2004; Lee et al., 1997; Chen et al., 1997; Arnfield et al., 1993)
WST09 (Tookad)	palladium-metalated bacteriopheophorbide MW 714		763	~0.1-0.25	~2 h	(Weersink et al., 2005b; Weersink et al., 2005a)

Photosensitizer (trade name)	Chemical Structure	Approval	λ_{ex} (nm)	DLI[1] (h)	Clearance Time	References
WST11	Palladium bacteriochlorin 130-(2-sulfoethyl) amide dipotassium salt MW 940		752	~0.1–0.25	~ 1 h	(Mazor et al., 2005)
Talaporfin sodium (LS11)	mono-L-aspartyl chlorin e_6 MW 711.8		664	1	14 days	(Lustig et al., 2003; Spikes and Bommer, 1993a; Kato et al., 2003)
Pc-4	silicon phthalocyanine MW 719.94		672	24–36	~ 28 h	(Baron et al., 2010; Miller et al., 2007; Kinsella et al., 2011)

[1]DLI: drug-light interval.

Table 5a

Clinically relevant photosensitizers and their photophysical parameters for FDA or EU approved photosensitizers. Each parameter is given a default value first, which is the *in-vivo* value consistent between parameters used in the table. A range for each parameter is provided next, mostly based on *in-vitro* measurement from literature. References, whenever existed, are provided for each parameter. When a parameter does not exist in the literature but can be estimated based on our review, it is presented in parenthesis. We use a "—" to represent parameters that are unknown at the time of the review.

Parameter	ALA-PpIX	BPD	mTHPC	Photofrin
e (cm^{-1}μM^{-1})	0.003 @633nm (Liu *et al.*, 2012; Lovell *et al*, 2010)	0.0783 @690nm (Aveline *et al.*, 1994; Zhu *et al.*, 2014)	0.111 @650nm (Johansson *et al.*, 2006)	0.0035 @630nm (Bonnet *et al.*, 1983; Zhu *et al.*, 2014)
k_0 @100mW/cm^2 (s^{-1})	1.59 [1]	45.13 [1]	60.27 [1]	1.84 [1]
k_1 (μM^{-1}s^{-1})	9×10^2 [2] (0.85 – 900) (Cox and Whitten, 1982; Georgakoudi and Foster, 1998)	1.7×10^2 [2] (150-550) (Kim *et al.*, 2014a; McMillan *et al.*, 2013)	2.97×10^2 [2] 12–297 (Dysart *et al.*, 2005; Mitra and Foster, 2005)	7.6×10^2 [2] (Georgakoudi *et al.*, 1997)
k_2 (μM^{-1}s^{-1})	1.9×10^3 (1700 – 2100) (Jarvi *et al.*, 2011)	3×10^3 (Aveline *et al.*, 1994)	2.6×10^3 (2500 – 2700) (Jarvi *et al.*, 2011)	1.4×10^3 (Sterenborg and van Gemert, 1996)
k_3 (s^{-1})	2.9×10^7 [3] (Sterenborg and van Gemert, 1996)	4.04×10^7 [4] (Aveline *et al.*, 1994)	1.47×10^7 [4]	2.9×107 (Sterenborg and van Gemert, 1996)
k_4 (s^{-1})	2.3×10^4 [5] (3.5×10^3 – 2.3×10^4)	3.6×10^4 [5]	2.3×10^4 [5] (0.9×10^4 – 2.3×10^4)	1.67×10^4 [5]
k_5 (s^{-1})	1.2×10^7 [6]	1.52×10^7 [6]	1.19×10^8 [6]	4.94×10^7 [6]
k_6 (s^{-1})	3.3×10^5 [7]	3.3×10^5 [7]	3.3×10^5 [7]	3.3×10^5 [7]
$k_7[A]$ (s^{-1})	1×10^7 [8] (3×10^6 – 3×10^7)	1×10^7 [8] (3×10^6 – 3×10^7)	1×10^7 [8] (3×10^6 – 3×10^7)	1×10^7 [8] (3×10^6 – 3×10^7)
$k_8[A]$ (s^{-1})	(0) [9]	(0) [9]	(0) [9]	(0) [9]
β (μM)	(11.9) [3]	(11.9) [3]	8.7 (Mitra and Foster, 2005)	11.9 (Georgakoudi *et al.*, 1997)
δ (μM)	(33) [3] (33 – 150) (Dysart *et al.*, 2005; Liu *et al.*, 2012)	(33) [3] (33 – 260) (Weston and Patterson, 2011)	(33) [3] (33 – 150) (Mitra and Foster, 2005)	33 (33 – 150) (Dysart *et al.*, 2005)
ξ (cm^{2}mW^{-1}s^{-1})	3.7×10^{-5} [3]	$(51 \pm 15) \times 10^{-3}$ (Kim *et al.*, 2014a; McMillan *et al.*, 2013)	30×10^{-3} (Mitra and Foster, 2005; Zhu *et al.*, 2015a)	3.7×10^{-3} (2.9 – 3.7) $\times 10^{-3}$ (Georgakoudi *et al.*, 1997; Mitra and Foster, 2005; Zhu *et al.*, 2014)
σ (μM^{-1})	$(9.0 \pm 1.6) \times 10^{-5}$ (Zhu *et al.*, 2015a; Georgakoudi and Foster, 1998) (2.8×10^{-8} – 9×10^{-5}) [9]	1.7×10^{-5} ($(1 – 5) \times 10^{-5}$) (Kim *et al.*, 2014a; McMillan *et al.*, 2013)	$(2.97 \pm 0.46) \times 10^{-5}$ (1.2 – 1.7) $\times 10^{-6}$ (Zhu *et al.*, 2015a; Mitra and Foster, 2005)	7.6×10^{-5} (Georgakoudi *et al.*, 1997)
η (cm^{2}mW^{-1}s^{-1} μM)	(0) [9]	(0) [9]	(0) [9]	(0) [9]
g (μM s^{-1})	—	1.7 ± 0.7 [7] (Kim *et al.*, 2014a; McMillan *et al.*, 2013)	—	0.76 (Wang *et al.*, 2010)
S_Δ	0.281 [10]	0.144 [10]	0.104 [10]	0.319 [10]
Φ_t	0.83 (Josefsen and Boyle, 2008)	0.79 (Aveline *et al.*, 1994)	0.89 (Mitra and Foster, 2005)	0.63 (0.63 – 0.80) (Mitra and Foster, 2005; Foster *et al.*, 1991; Zhu *et al.*, 2014)

Parameter	ALA-PpIX	BPD	mTHPC	Photofrin
Φ_Δ	0.233 [11] (0.54 – 0.77) (Cox *et al.*, 1982; Redmond and Gamlin, 1999)	0.114 [11] (0.17–0.84) (Fernandez *et al.*, 1997; Redmond and Gamlin, 1999)	0.093 [11] (0.3-0.43) (Hadjur *et al*, 1998; Dysart *et al.*, 2005)	0.20 [11] (0.12-0.56) (Mitra and Foster, 2005; Lovell *et al.*, 2010)
Φ_f	0.16 [3]	0.05 (Aveline *et al.*, 1994)	0.14 (Milanesio *et al.*, 2001)	0.16 (Redmond and Gamlin, 1999)
τ_f (s)	$(6.3\pm1.2)\times10^{-9}$ (Russell *et al.*, 2008)	5.2×10^{-9} (Aveline *et al.*, 1994)	7.5×10^{-9} (Kress *et al.*, 2003)	$(5.5\pm1.2)\times10^{-9}$ (Russell *et al.*, 2008)

[1] Calculated based on value of ε and $\phi = 100$ mW/cm^2: $k_0 = \varepsilon\phi/(h\nu)$)

ALA-PPIX: $k_0 = (0.003\ \mu M^{-1}cm^{-1})/(6.022\times10^{14}\ m^2\mu M^{-1}) \times (100\ mW/cm^2)/(3.14\times10^{-16}\ mW\ s) = 1.59\ s^{-1}$

BPD: $k_0 = (0.0783\ \mu M^{-1}cm^{-1})/(6.022\times10^{14}\ cm^2\mu M^{-1}) \times (100\ mW/cm^2)/(2.88\times10^{-16}\ mW\ s) = 45.13\ s^{-1}$

mTHPC: $k_0 = (0.111\ \mu M^{-1}cm^{-1})/(6.022\times10^{14}\ cm^2\mu M^{-1}) \times (100\ mW/cm^2)/(3.06\times10^{-16}\ mW\ s) = 60.27\ s^{-1}$

Photofrin: $k_0 = (0.0035\ \mu M^{-1}cm^{-1})/(6.022\times10^{14}\ cm^2\mu M^{-1}) \times (100\ mW/cm^2)/(3.16\times10^{-16}\ mW\ s) = 1.84\ s^{-1}$

[2] Calculated based on value of σ and k_7: $k_1 = \sigma \times k_7[A]$

ALA-PPIX: $k_1 = (9\times10^{-5}\ \mu M^{-1}) \times (1\times10^7\ s^{-1}) = 9\times10^2\ \mu M^{-1}s^{-1}$

BPD: $k_1 = (1.7\times10^{-5}\ \mu M^{-1}) \times (1\times10^7\ s^{-1}) = 1.7\times10^2\ \mu M^{-1}s^{-1}$

mTHPC: $k_1 = (2.97\times10^{-5}\ \mu M^{-1}) \times (1\times10^7\ s^{-1}) = 2.97\times10^2\ \mu M^1 s^1$

Photofrin: $k_1 = (7.6\times10^{-5}\ \mu M^{-1}) \times (1\times10^7\ s^{-1}) = 7.6\times10^2\ \mu M^{-1}s^{-1}$

[3] Assumed to be the same as that of Photofrin.

[4] Calculated based on the value of Φ_t and τ_f: $k_3 = (1 - \Phi_t)/\tau_f$

BPD: $k_3 = (1 - 0.79)/(5.2\times10^{-9}\ s) = 4.04\times10^7\ s^{-1}$

mTHPC: $k_3 = (1 - 0.89)/(7.5\times10^{-9}\ s) = 1.47\times10^7\ s^{-1}$

[5] Calculated based on value of β and k_2: $k_4 = \beta \times k_2$

ALA-PPIX: $k_4 = (11.9\ \mu M) \times (1.9\times10^3\ \mu M^{-1}s^{-1}) = 2.3\times10^4\ s^{-1}$

BPD: $k_4 = (11.9\ \mu M) \times (3\times10^3\ \mu M^{-1}s^{-1}) = 3.6\times10^4\ s^{-1}$

mTHPC: $k_4 = (8.7\ \mu M) \times (2.6\times10^3\ \mu M^{-1}s^{-1}) = 2.3\times10^4\ s^{-1}$

Photofrin: $k_4 = (11.9\ \mu M) \times (1.4\times10^3\ \mu M^{-1}s^{-1}) = 1.67\times10^4\ s^{-1}$

[6] Calculated based on value of k_3 and Φ_f: $k_5 = \Phi_t k/(1 - \Phi_t)$

ALA-PPIX: $k_5 = (0.83) \times 2.9\times10^7\ s^1/(1 - 0.83) = 1.2\times10^7\ s^{-1}$

BPD: $k_5 = (0.79) \times 4.04\times10^7\ s^{-1}/(1 - 0.79) = 1.52\times10^7\ s^{-1}$

mTHPC: $k_5 = (0.89) \times 1.47\times10^7\ s^{-1}/(1 - 0.89) = 1.19\times10^7\ s^{-1}$

Photofrin: $k_5 = (0.63) \times 2.9\times10^7\ s^{-1}/(1 - 0.63) = 4.94\times10^7\ s^{-1}$

[7] $\tau_\Delta = 3$ μs in water and 0.16 μs in tissue (Dysart et al., 2005). $k_6 = \tau_\Delta^{-1} - k_7[A] = (3\ \mu s)^{-1} = 3.3\times10^5\ s^{-1}$

[8] $k_7[A] = \tau_\Delta^{-1} - k_6 = (0.1\ \mu s)^{-1} - (3.3\times10^5\ s^{-1}) = 1\times10^7\ s^{-1}$, taken from (Zhu *et al.*, 2015b).

[9] Assume no hypoxic interaction.

[10] *In-vivo* values calculated based on the values of ξ, Φ_t, and ε: $S_\Delta = \xi/\Phi_t/\varepsilon\ (h\nu)$

ALA-PPIX: $S_\Delta = (3.7\times10^{-3}\ cm^2mW^{-1}s^{-1})/(0.83)/(0.003\ \mu M^{-1}cm^{-1}) \times (6.022\times10^{14}\ cm^3\mu M^{-1}) \times (3.14\times10^{-16}\ mW\ s) = 0.281$

BPD: $S_\Delta = (5\ 1\times10^{-3}\ cm^2mW^{-1}s^{-1})/(0.79)/(0.0312\ \mu M^1cm^{-1}) \times (6.022\times10^{14}\ cm^3\mu M^{-1}) \times (2.72\times10^{-16}\ mW\ s) = 0.144$

mTHPC: $S_\Delta = (30\times10^{-3}\ cm^2mW^{-1}s^{-1})/(0.89)/(0.111\ \mu M^{-1}cm^{-1}) \times (6.022\times10^{14}\ cm^3\mu M^{-1}) \times (3.06\times10^{16}\ mW\ s) = 0.056$

Photofrin: $S_\Delta = (3.7 \times 10^{-3} \text{ cm}^2\text{mW}^{-1}\text{s}^{-1})/(0.63)/(0.0035 \text{ μM}^{-1}\text{cm}^{-1}) \times (6.022 \times 10^{14} \text{ cm}^3\text{μM}^{-1}) \times (3.16 \times 10^{-16} \text{ mW s}) = 0.319$

[11]*In-vivo* values calculated based on the values of S_Δ and Φ_t. $\Phi_\Delta = S_\Delta \times \Phi_t$

ALA-PPIX: $\Phi_\Delta = (0.281) \times (0.83) = 0.233$

BPD: $\Phi_\Delta = (0.144) \times (0.83) = 0.114$

mTHPC: $\Phi_\Delta = (0.104) \times (0.89) = 0.093$

Photofrin: $\Phi_\Delta = (0.319) \times (0.63) = 0.20$

Table 5b

Clinically relevant photosensitizers and their photophysical parameters for non-FDA or non-EU approved but common photosensitizers. Each parameter is given a default value first, which is the *in-vivo* value consistent between parameters used in the table. A range for each parameter is provided next, mostly based on *in-vitro* measurement from literature. References, whenever existed, are provided for each parameter. When a parameter does not exist in the literature but can be estimated based on our review, it is presented in parenthesis. We use a "—" to represent parameters that are unknown at the time of the review.

Parameter	HPPH	LS11	mLu	Pc 4	WST09	WST11
ε (μM⁻¹cm⁻¹)	0.109 @665nm (Bellnier et al., 2003)	0.040 @654nm (Spikes and Bommer, 1993b)	0.0312 @732nm (Zhu et al., 2003)	0.200 @675nm (Baron et al., 2010)	0.09296 @762nm (Weersink et al., 2005b)	0.12 @ 752 nm (Price et al., 2013)
k_0 @ 100 mW/cm² (s⁻¹)	60.55 [1]	21.85 [1]	19.08 [1]	112.78 [1]	59.17 [1]	75.39 [1]
k_1 (μM⁻¹s⁻¹)	1×10² [2]	1.14×10⁴ [3] (Spikes and Bommer, 1993a)	(~1×10²) [4]	—	(1.6×10²) [5]	1.6×10² [6]
k_2 (μM⁻¹s⁻¹)	3×10³ (2.5 – 3.4)×10³ (Pandey et al., 1996)	1.9×10³ (1.3 – 1.9)×10³ (Spikes and Bommer, 1993b)	1.3×10³ (Guldi et al., 2000)	3.83×10³ (He et al., 1997)	2.2×10³ (Vakrat-Haglili et al., 2005)	(~2.2×10³) [7]
k_3 (s⁻¹)	(8×10⁶) [8]	6.0×10⁷ [8]	1.58×10⁹ [8]	(1×10⁸) [8]	1.7×10¹⁰ (Vakrat-Haglili et al., 2005)	(1.7×10¹⁰) [7]
k_4 (s⁻¹)	3.6 ×10⁴ [9]	1.4×10⁴ (1.4 – 1.9) ×10⁴ (Ohmori et al., 2007)	1.5×10⁴ [9]	4.6×10⁴ [9]	2.6×10⁴ [9]	(~2.6×10⁴) [7]
k_5 (s⁻¹)	(1.92×10⁸) [10]	2.4×10⁸ [10]	8.31×10⁸ [10]	(1×10⁸) [10]	8.33×10¹¹ [10]	(~8.33×10¹¹) [7]
k_6 (s⁻¹)	3.3×10⁵ [11]	3.3×10⁵ [11]	3.3×10⁵ [11]	3.3×10⁵ [11]	3.3×10⁵ [11]	3.3×10⁵ [11]
$k_7[A]$ (s⁻¹)	1×10⁷ [12] (3×10⁶ – 3×10⁷)	1×10⁷ [12] (3×10⁶ – 3×10⁷)	1×10⁷ [12] (3×10⁶ – 3×10⁷)	1×10⁷ [12] (3×10⁶ – 3×10⁷)	(1×10⁷) [13] (3×10⁶ – 3×10⁷)	(1×10⁷) [13] (3×10⁶ – 3×10⁷)
$k_8[A]$ (s⁻¹)	(0) [14]	(0) [14]	(0) [14]	(0) [14]	—	—
β (μM)	(11.9) [15]	7.4 [16]	(11.9) [15]	(11.9) [15]	(11.9) [15]	(11.9) [15]
δ (μM)	(33) [15]	(33) [15]	(33) [15]	(33) [15]	(33) [15]	(33) [15]
ξ (cm²mW⁻¹s⁻¹)	(70±40)×10⁻³ (Penjweini et al., 2015b)	(36.8×10⁻³) [17]	(13.8×10⁻³) [17]	(118.7×10⁻³) [17]	122×10⁻³ [18]	(155.5×10⁻³) [18]
σ (μM⁻¹)	1±6×10⁻⁵ (Penjweini et al., 2015b)	1.14×10⁻³ [19]	1×10⁻⁵ [19]	—	1.6×10⁻⁵ [19]	(1.6×10⁻⁵) [7]
η (cm²mW⁻¹s⁻¹ μM)	(0) [14]	(0) [14]	(0) [14]	(0) [14]	—	—
g (μM s⁻¹)	1.5±0.9 (Penjweini et al., 2015b)	—	—	—	—	—

Parameter	HPPH	LS11	mLu	Pc 4	WST09	WST11
S_Δ or S_1	0.12 [20]	(0.211) [20]	(0.211) [20]	(0.211) [20]	0.211 [20]	(0.211) [7]
Φ_t	0.96 0.48 – 1 (Bellnier et al., 2003)	0.8 >0.8 (Ohmori and Arai, 2006)	0.344 (Guldi et al., 2000)	(~0.5) [21]	0.98 (Weersink et al., 2005b)	(0.98) [7]
Φ_Δ or Φ_{ROS}	0.12 [22] 0.48 (Bellnier et al., 2003)	0.17 [22] 0.77 (Spikes and Bommer, 1993b) (0.61 – 0.77)	0.073 [22] 0.31 (Guldi et al., 2000)	0.11 [22] 0.43 (He et al., 1997)	0.21 [22] 0.1 - 1 (Ormond and S.., 2013; Vakrat-Haglili et al., 2005)	(0.21) [7]
Φ_f	0.43 (Pandey et al., 1996)	0.008 – 0.010 (Li et al., 2002)	0.01 – 0.015 (Guldi et al., 2000; Lovell et al., 2010)	0.62 – 0.8 (Nyokong, 2007)	(<0.01) [23]	(<0.01) [23]
τ_f(s)	(~5x10⁻⁹) [24]	(3.3–3.8)×10⁻⁹ (Li et al., 2002)	4.14×10⁻¹⁰ (Guldi et al., 2000)	(4.59±0.03)×10⁻⁹ (Zhao et al., 2009)	12×10⁻¹² [25]	(1.2×10⁻¹²) [7]

[1] Calculated based on value of e and ϕ = 100 mW/cm². $k_0 = e\phi/(h\nu)$

HPPH: $k_0 = (0.109 \mu M^{-1} cm^{-1})/(6.022\times10^{14} cm^3 \mu M^{-1}) \times (100\ mW/cm^2)/(2.99\times10^{-16}\ mW\ s) = 60.55\ s^{-1}$

LS11: $k_0 = (0.040\ \mu M^{-1} cm^{-1})/(6.022\times 10^{14} cm^3 \mu M^{-1}) \times (100\ mW/cm^2)/(3.04 \times 10^{-16}\ mW\ s) = 21.85\ s^{-1}$

mLu: $k_0 = (0.0312\ \mu M^{-1} cm^{-1})/(6.022\times 10^{14} cm^3 \mu M^{-1}) \times (100\ mW/cm^2)/(2.72 \times 10^{-16}\ mW\ s) = 19.08\ s^{-1}$

Pc 4: $k_0 = (0.200\ \mu M^{-1} cm^{-1})/(6.022\times 10^{14} cm^3 \mu M^{-1}) \times (100\ mW/cm^2)/(2.94 \times 10^{-16}\ mW\ s) = 112.78\ s^{-1}$

WST09: $k_0 = (0.09296\ \mu M^{-1} cm^{-1})/(6.022\times10^{14} cm^3 \mu M^{-1}) \times (100\ mW/cm^2)/(2.61 \times10^{-16}\ mW\ s) = 59.17\ s^{-1}$

WST11: $k_0 = (0.12\ \mu M^{-1} cm^{-1})/(6.022\times10^{14} cm^3 \mu M^{-1}) \times (100\ mW/cm^2)/(2.64 \times10^{-16}\ mW\ s) = 75.39\ s^{-1}$

[2] Calculated based on value of σ and k_7. $k_1 = \sigma \times k_7[A]$

HPPH: $k_1 = (1\times10^{-5}\ \mu M^{-1}) \times (1\times10^7\ s^{-1}) = 1\times10^2\ \mu M^{-1} s^{-1}$

[3] Calculated based on quantum yield of photobleaching being 15 times larger than that of Photofrin (Spikes and Bommer, 1993a)

[4] Assumed value to be in the same order of magnitude as that of HPPH due to the low photobleaching characteristics

[5] Assumed to be the same as that of WST11

[6] Calculated based on analysis of photobleaching data from (Price et al., 2013)

[7] Assumed to be the same as that of WST09 and all photosensitizers having values of the same order of magnitude

[8] Calculated based on the value of Φ_f and τ_f. $k_3 = (1 - \Phi_f)/\tau_f$

HPPH: $k_3 = (1 - 0.96)/(5\times10^{-9}\ s) = 8\times10^6\ s^{-1}$

LS11: $k_3 = (1 - 0.8)/(3.3\times10^{-9}\ s) = 6\times10^7\ s^{-1}$

Mlu: $k_3 = (1 - 0.344)/(4.14\times10^{-10}\ s) = 1.58\times10^9\ s^{-1}$

PC4: $k_3 = (1 - 0.5)/(4.6\times10^{-9}\ s) = 1\times10^8\ s^{-1}$

[9] Calculated based on value of β and k_2, $k_4 = \beta \times k_2$

HPPH: $k_4 = (11.9 \ \mu M) \times (3 \times 10^3 \ \mu M^{-1}s^{-1}) = 3.6 \times 10^4 \ s^{-1}$

mLu: $k_4 = (11.9 \ \mu M) \times (1.3 \times 10^3 \ \mu M^{-1}s^{-1}) = 1.4 \times 10^4 \ s^{-1}$

Pc 4: $k_4 = (11.9 \ \mu M) \times (3.83 \times 10^3 \ \mu M^{-1}s^{-1}) = 4.6 \times 10^4 \ s^{-1}$

WST09: $k_4 = (11.9 \ \mu M) \times (2.2 \times 10^3 \ \mu M^{-1}s^{-1}) = 2.6 \times 10^4 \ s^{-1}$

[10] Calculated based on value of k_3 and Φ_t, $k_5 = \Phi_t k/(1 - \Phi_v)$

HPPH: $k_5 = (0.96) \times (8 \times 10^6 \ s^{-1})/(1 - 0.96) = 1.92 \times 10^8 \ s^{-1}$

LS11: $k_5 = (0.8) \times (6 \times 10^7 \ s^{-1})/(1 - 0.8) = 2.4 \times 10^8 \ s^{-1}$

mLu: $k_5 = (0.344) \times (1.58 \times 10^9 \ s^{-1})/(1 - 0.344) = 8.31 \times 10^8 \ s^{-1}$

Pc4: $k_5 = (0.5) \times (1 \times 10^8 \ s^{-1})/(1 - 0.5) = 1 \times 10^8 \ s^{-1}$

WST09: $k_5 = (0.98) \times (1.7 \times 10^{10} \ s^{-1})/(1 - 0.98) = 8.33 \times 10^{11} \ s^{-1}$

[11] $\tau_\Delta = 3$ μs in water and 0.16 μs in tissue (Dysart et al., 2005). $k_6 = \tau_\Delta^{-1} - k_7[A] = (3 \ \mu s)^{-1} = 3.3 \times 10^5 \ s^{-1}$

[12] $k_7[A] = \tau_\Delta^{-1} - k_6 = (0.1 \ \mu s)^{-1} - (3.3 \times 10^5 \ s^{-1}) = 1 \times 10^7 \ s^{-1}$, taken from (Zhu et al., 2015b).

[13] Assume tissue damage due to type I action is the same as that due to type II action, i.e., $k_{71}[A] = k_{72}[A]$.

[14] Assume no hypoxic interaction.

[15] Assumed to be similar to values for Photofrin

[16] Calculated based on value of k_2 and k_4 $\beta = k_4/k_2 = (1.4 \times 10^4 \ s^{-1})/(1.9 \times 10^3 \ \mu M^{-1}s^{-1}) = 7.4 \ \mu M$

[17] Calculated based on value of ξ for Photofrin: $\xi = \xi_{phot} \times (e/e_{phot}) \times (h\nu_{pho}/h\nu) \times (\Phi_t/\Phi_{t\_phot}) \times (0.66)$ where 0.66 is the average value of $\xi_{experimental}/\xi_{calculated}$ for Photofrin, ALA, BPD, mTHPC, and HPPH

LS11: $\xi = (3.7 \times 10^{-3} \ cm^2 \ mW^{-1}s^{-1}) \times (0.04 \ \mu M^{-1}cm^{-1}/0.0035 \ \mu M^{-1}cm^{-1}) \times (3.16 \times 10^{-16} \ mW \ s/3.04 \times 10^{-16} \ mW \ s) \times (0.8/0.63) \times 0.66 = 36.8 \times 10^{-3} \ cm^2 \ mW^{-1}s^{-1}$

mLu: $\xi = (3.7 \times 10^{-3} \ cm^2 \ mW^{-1}s^{-1}) \times (0.0312 \ \mu M^{-1}cm^{-1}/0.0035 \ \mu M^{-1}cm^{-1}) \times (3.16 \times 10^{-16} \ mW \ s/2.72 \times 10^{-16} \ mW \ s) \times (0.344/0.63) \times 0.66 = 13.8 \times 10^{-3} \ cm^2 \ mW^{-1}s^{-1}$

Pc4: $\xi = (3.7 \times 10^{-3} \ cm^2 \ mW^{-1}s^{-1}) \times (0.200 \ \mu M^{-1}cm^{-1}/0.0035 \ \mu M^{-1}cm^{-1}) \times (3.16 \times 10^{-16} \ mW \ s/2.94 \times 10^{-16} \ mW \ s) \times (0.5/0.63) \times 0.66 = 118.7 \times 10^{-3} \ cm^2 \ mW^{-1}s^{-1}$, where the value of Φ_t was assumed to be 0.5

[18] Calculated based on value of ξ for Photofrin: $\xi = \xi_{phot} \times (e/e_{phot}) \times (h\nu_{pho}/h\nu) \times (\Phi_t/\Phi_{t\_phot}) \times (0.66)$ where 0.66 is the average value of $\xi_{experimental}/\xi_{calculated}$ for Photofrin, ALA, BPD, mTHPC, and HPPH. Notice that ξ here is due to type I interaction, S_I, rather than type II interaction, S_Δ. We have assumed $S_I/S_\Delta = 0.66$ between WST09 (or WST11) and Photofrin.

WST09: $\xi = (3.7 \times 10^{-3} \ cm^2 \ mW^{-1}s^{-1}) \times (0.09296 \ \mu M^{-1}cm^{-1}/0.0035 \ \mu M^{-1}cm^{-1}) \times (3.16 \times 10^{16} \ mW \ s/2.61 \times 10^{-16} \ mW \ s) \times (0.98/0.63) \times 0.66 = 122 \times 10^{-3} \ cm^2 \ mW^{-1}s^{-1}$

WST11: $\xi = (3.7 \times 10^{-3} \ cm^2 \ mW^{-1}s^{-1}) \times (0.12 \ \mu M^{-1}cm^{-1}/0.0035 \ \mu M^{-1}cm^{-1}) \times (3.16 \times 10^{-16} \ mW \ s/2.64 \times 10^{-16} \ mW \ s) \times (0.98/0.63) \times 0.66 = 155.5 \times 10^{-3} \ cm^2 \ mW^{-1}s^{-1}$

[19] Calculated based on value of k_1 and $k_7[A]$; $\sigma = k_1/k_7[A]$

LS11: $\sigma = (1.4 \times 10^4 \ \mu M^{-1}s^{-1})/(1 \times 10^7 \ s^{-1}) = 1.14 \times 10^{-3} \ \mu M^{-1}$

WST09: $\sigma = (1.6 \times 10^2 \ \mu M^{-1}s^{-1})/(1 \times 10^7 \ s^{-1}) = 1.6 \times 10^{-5} \ \mu M^{-1}$

MLu: $\sigma = (1 \times 10^2 \; \mu M^{-1} s^{-1})/(1 \times 10^7 \; s^{-1}) = 1 \times 10^{-5} \; \mu M^{-1}$

[20] Calculated based on the values of ξ, Φ_t, and ε: $S_\Delta = \xi \Phi_t/\varepsilon \times(h\nu)$ for type II or $S_I = \xi \Phi_t/\varepsilon \times(h\nu)$ for type I.

LS11: $S_\Delta = (36.8 \times 10^{-3} \; cm^2 mW^{-1} s^{-1})/(0.8)/(0.04 \; \mu M^{-1} cm^{-1}) \times (6.022 \times 10^{14} \; cm^3 \mu M^{-1}) \times (3.04 \times 10^{-16} mW \; s) = 0.211$

mLu: $S_\Delta = (13.8 \times 10^{-3} \; cm^2 mW^{-1} s^{-1})/(0.344)/(0.0312 \; \mu M^{-1} cm^{-1}) \times (6.022 \times 10^{14} \; cm^3 \mu M^{-1}) \times (2.72 \times 10^{-16} mW \; s) = 0.211$ WST09: $S_I = (122 \times 10^{-3} \; cm^2 mW^{-1} s^{-1})/(0.98)/(0.09296 \; \mu M^{-1} cm^{-1}) \times (6.022 \times 10^{14} \; cm^3 \mu M^{-1}) \times (2.61 \times 10^{-16} mW \; s) = 0.211$

[21] Assumed value of Φ_t that is of the same order of magnitude as that of other photosensitizers to be used in calculations

[22] In-vivo values calculated based on the values of S_Δ (or S_I) and Φ_t: $\Phi_\Delta = S_\Delta \times \Phi_t$ for type II or $\Phi_{ROS} = S_I \times \Phi_t$ for type I. HPPH: $\Phi_\Delta = (0.12) \times (0.96) = 0.12$ LS11: $\Phi_\Delta = (0.211) \times (0.8) = 0.17$ mLu:
$\Phi_\Delta = (0.211) \times (0.344) = 0.073$
Pc 4: $\Phi_\Delta = (0.211) \times (0.5) = 0.11$
WST09: $\Phi_{ROS} = (0.211) \times (0.98) = 0.21$

[23] Assumed to be <0.01 due to the lack of fluorescence signal for WST09 and WST11 (Vakrat-Haglili et al., 2005)

[24] Assumed value to be in the same order of magnitude as other type II photosensitizers.

[25] Calculated based on value of k_3 and k_5: $\tau_f = 1/(k_3 + k_5)$
WST-09: $\tau_f = 1/(1.7 + 83.3) \times 10^{10} \; s^{-1} = 1.2 \times 10^{-12} \; s$